R&D of Beam Monitors at J-PARC Neutrino Beamline

Ryosuke Ishida
Department of Physics, University of Tokyo

February 3, 2005

Abstract

The T2K experiment is a next generation long baseline neutrino oscillation experiment following the current ongoing K2K experiment in Japan. A high intensity narrow band neutrino beam is produced by a high intensity proton beam. The power of the proton beam in T2K is more than 100 times higher than that in K2K. The superconducting magnets are used to bend the 50GeV proton beam about 80 degrees toward the Super-Kamiokande. To protect the superconducting magnets from quenching, we should control the proton beam precisely. It is also important to keep the proper beam size not to destroy the target. We have to establish the beam tuning scheme with beam monitors.

We have carried out the beamline simulations based on Geant4. We check the number and positions of beam monitors to tune the proton beam, and study the emittance measurement scheme.

We also study the feasibility of the Residual Gas Beam Profile Monitor (RGBPM) as a proton beam monitor candidate for the J-PARC neutrino beamline. To check the basic performance, we have carried out beam tests at the K2K neutrino beamline and the NML beamline at KEK-PS. We find it is difficult to operate RGBPM under the high beam-induced background environment and high beam-induced electric field.

Contents

List of Figures

List of Tables

Chapter 1

Introduction

Neutrinos were considered as massless particles since their observation in 1956. At Super-Kamiokande in 1998, a flavor oscillation in the atmospheric neutrino was observed[1], which proved the finite masses of neutrinos. The oscillation parameters, mixing angle of neutrino, were also measured.

To confirm the results of the neutrino oscillation, the KEK to Kamioka (K2K) long baseline neutrino oscillation experiment has been carried out since 1999. In this experiment, muon neutrino beam is produced at the KEK-PS and is detected by Super-Kamiokande. The disappearance of the muon neutrinos, the neutrino oscillation to other flavors of neutrinos, is observed in the experiment[2]. The results are consistent to that of the atmospheric neutrino experiment.

The statistics, however, is not sufficient to decide the oscillation parameters precisely. For the precise measurement to determine the oscillation parameters and a search for a new physics, it is necessary to produce a higher intensity neutrino beam than that of the K2K experiment to get the larger statistics. The Tokai to Kamioka (T2K) long baseline neutrino oscillation experiment, which is a next generation neutrino oscillation experiment, produces a much higher intensity neutrino beam using the J-PARC proton synchrotron accelerator.

The J-PARC proton synchrotron has 100 times higher beam power than KEK-PS. To control and deliver such a high power proton beam to the neutrino production target, there exist some difficulties: we must avoid quenching of the superconducting magnets, must protect the target, and so on. To control the proton beam precisely, several kinds of beam monitors are going to be installed in the neutrino beamline. We have developed the one of the beam monitors, the Residual Gas Beam Profile Monitor (RGBPM) for the neutrino beamline. We have also established the proton delivery scheme.

In this thesis, we present the overview of the T2K experiment in Chapter 2, the J-PARC neutrino beamline in Chapter 3, the study of the beam monitoring scheme in Chapter 4, and the R&D of the RGBPM in Chapter5.

Chapter 2

T2K Long Baseline Neutrino Oscillation Experiment

2.1 Overview

The T2K experiment is the next generation long baseline neutrino oscillation experiment following the K2K experiment that is the ongoing experiment, in Japan. In T2K, a muon neutrino beam is produced at the J-PARC 50GeV proton synchrotron in Tokai, and is detected by the Super-Kamiokande in Kamioka. (See Fig.2.1.) The baseline length is about 295km.

Figure 2.1: Overview of the T2K experiment

The proton accelerator at J-PARC has 50 times higher intensity and more than 100 times higher beam power than KEK-PS. Also the neutrino beam has very high intensity and it provides more precise measurements of the neutrino oscillation parameters than the K2K results. The precise measurement of the neutrino oscillation is one of the keys to reveal the origin of mass and the origin of material in the Universe.

The neutrino oscillation probability relevant to the experiment can be expressed by the following formula:

$$P(\nu_\mu \to \nu_\mu) \sim 1 - \sin^2 2\theta_{23} \sin^2 \Phi_{23}, \tag{2.1}$$
$$P(\nu_\mu \to \nu_e) \sim \sin^2 \theta_{13} \sin^2 \Phi_{23}, \tag{2.2}$$

where

$$\Phi_{23} = 1.27\Delta m^2_{23}[\mathrm{eV}^2]L[\mathrm{km}]/E_\nu[\mathrm{GeV}]$$

gives oscillation pattern depending on the baseline length L and the neutrino energy E_ν. Δm^2_{23} is measured to be about $3 \times 10^{-3}[\mathrm{eV}^2]$ in the former experiments. (See Appendix A.) By yielding the distance from Tokai to Kamioka to L, the energy to make the neutrino oscillation maximum becomes about 0.7GeV. We, therefore, adjust the peak energy of the neutrino beam to be about 0.7GeV by employing the off axis configuration shown in the next section.

The goals of this experiment at the first stage are:

- Discovery of $\nu_\mu \to \nu_e$ oscillation at $\Delta m^2 \sim 3 \times 10^{-3}\mathrm{eV}^2$ down to $\sin^2\theta_{13} \sim 0.006$. This is a factor of twenty improvement in sensitivity over the past experiment,
- Precise measurement of the oscillation parameters in ν_μ disappearance down to $\delta(\Delta m^2) = 10^{-4}\mathrm{eV}^2$ and $\delta(\sin^2\theta_{23}) = 0.01$, and
- Search for a sterile component in ν_μ disappearance by the neutral current events measurement.

After these goals are successfully achieved, we further proceed to the second stage of the experiment. In the second stage, CP violation in the lepton sector will be measured with the upgraded 4MW 50-GeV PS (5 times higher power) and with the 1 Mt Hyper-Kamiokande (20 times larger size than SK).

2.2 Neutrino Beam

The neutrino beam is produced with a conventional method. A proton beam is bombarded to the target to produce pions. Then, a muon neutrino beam is produced by the pions' decay.

2.2.1 Off Axis Beam

We adopt an off axis beam (OAB) configuration. The OAB is the method to obtain the narrow neutrino energy spectrum. In the OAB method, the neutrino detectors are placed at a few degrees (Off-Axis angle) off from the beam axis as shown in Fig.2.2.

Since a pion decay is a two-body decay, the neutrino energy from the parent pion is the constant at the pion's rest frame. With a finite decay angle, the neutrino energy, therefore, becomes insensitive to the parent pion momentum as shown in Fig.2.3 and equation,

$$E_\nu = \frac{m_\pi^2 - m_\mu^2}{2(E_\pi - p_\pi \cos\theta)} \sim \frac{E_\pi(m_\pi^2 - m_\mu^2)}{m_\pi^2 + p_\pi^2 \sin^2\theta}. \tag{2.3}$$

The peak energy of the neutrino spectrum is set about 0.7GeV by choosing the off axis angle (2 to 3 degrees).

The advantages of the narrow neutrino energy spectrum are,

- to reduce the inelastic interactions of the high energy tail neutrinos which are misidentified as charged current quasi elastic (CCQE) events,
- to reduce the π_0 productions which are the large background of electron neutrino events, and
- to reduce the systematic error of the pion production uncertainty.

Adopting the OAB configuration, the total neutrino flux decreases, but the high power proton beam compensates the loss.

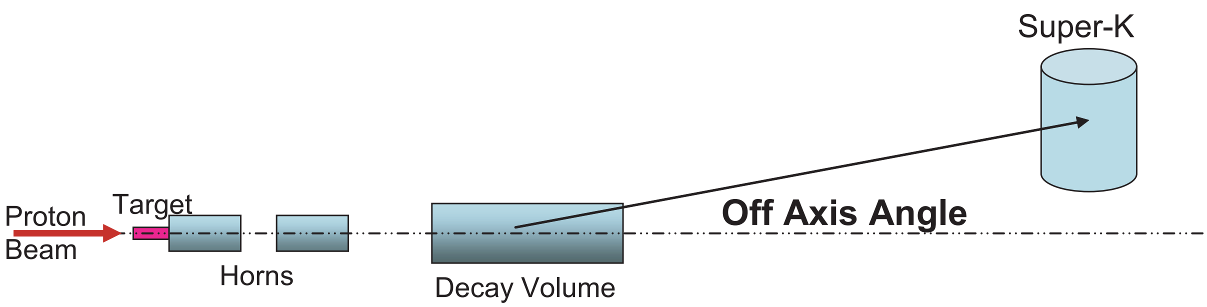

Figure 2.2: Overview of the off axis beam

2.3 J-PARC Accelerator and Fast extraction

The layout of the J-PARC facility is shown in Fig.2.4.

The J-PARC accelerator consists of the 400MeV Linac, the 3GeV Synchrotron (RCS:Rapid Cycling Synchrotron), and the 50GeV Synchrotron (50GeV-PS). In the 50GeV-PS, the expected intensity of the proton beam is 3.3×10^{14}ppp (protons per pulse) and the repetition rate is about 0.3Hz. The proton beam consists of 8 bunches and the beam is extracted to the neutrino beamline keeping the bunch structure. The beam pulse containing 8 bunches is called "*spill*". The beam structure is shown in Fig.2.5. The extraction scheme is called "*fast extraction*" and we can bombard the high intensity proton beam to the neutrino production target within very short time. The off-spill background is dramatically reduced due to the fast extraction. The accelerator parameters of the KEK-PS and the J-PARC PS are summarized in Table2.1.

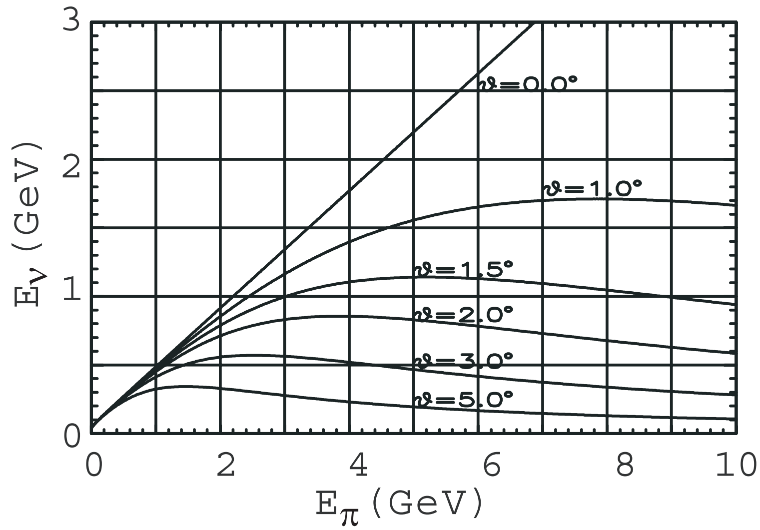

Figure 2.3: The energy distribution of neutrino at some off-axis angle

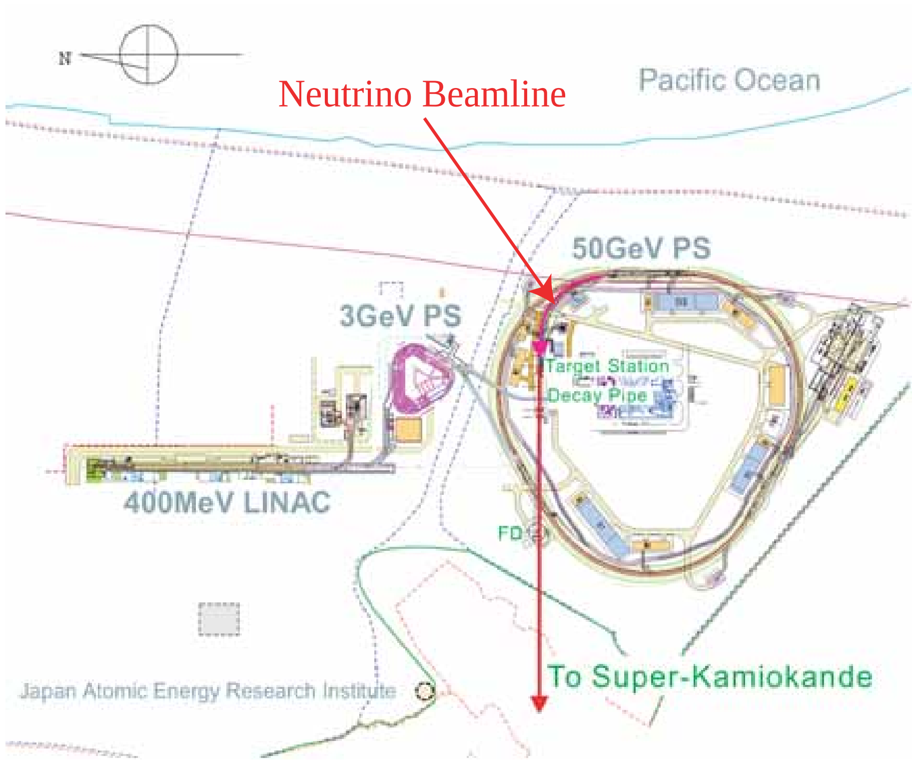

Figure 2.4: Overview of the J-PARC accelerator

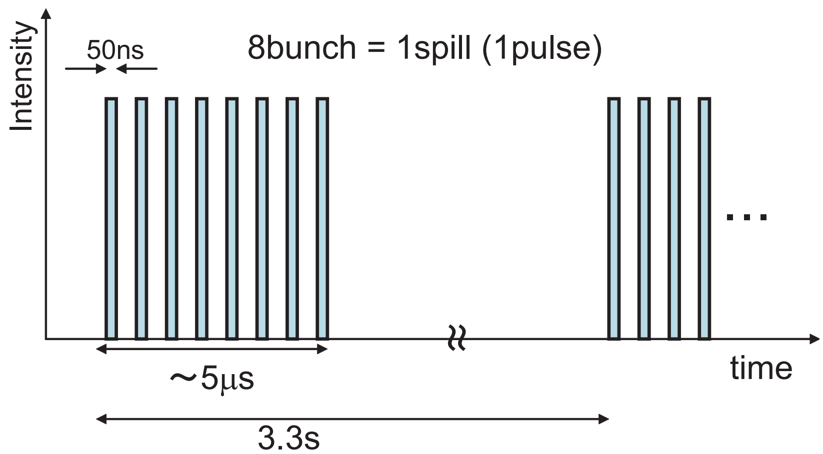

Figure 2.5: Bunch structure of the fast extracted beam to J-PARC neutrino beamline

	KEK-PS	J-PARC PS
Beam Energy [GeV]	12	50
Beam Intensity [ppp]	6.6×10^{12}	3.3×10^{14}
Repetition Rate [Hz]	0.46	0.28
Spill width [μs]	1.1	5
Number of bunches	9	8
Beam Power [MW]	0.0052	0.75

Table 2.1: Comparison of the proton accelerators for the neutrino experiments.

2.4 J-PARC Neutrino Facility

The proton beam extracted from the 50GeV PS to the neutrino beamline is bent by about 80 degrees toward Kamioka and transported to the target. We will describe the primary proton beamline in a latter chapter. The target is made of graphite and 3cm in diameter and 90cm in length. The proton beam hits the target and produces a number of pions and kaons by the hadronic interaction. The produced pions and kaons are focused toward SK by three toroidal horn magnets. In the horns, the positive charged hadrons are focused and the negative ones are spread. The pions and kaons decay into muons and muon neutrinos in the decay volume. After the decay volume, an iron and concrete beam dump stop all charged particles except high energy muons. The direction and the intensity of the muons are measured by a muon monitor to confirm the stability of the direction and the intensity of the neutrino beam.

2.5 Near neutrino detector

The produced neutrino beam is measured by the near neutrino detectors at 280m downstream from the target. One is set at the off axis degrees, and the other is set on the line of the proton beam. The purposes of these detectors are to measure the stability of neutrino beam direction, total flux, energy spectrum and electron neutrino contamination. These measured parameters are used to predict the neutrino flux and energy spectrum at Super-K without neutrino oscillation.

At the 280m detector, the shape of the neutrino spectrum is different from that at Super-K; the decay pipe, which is the neutrino source, has a finite length and the off-axis angle have a finite range for the 280m detector, while the length of the decay pipe is negligible for Super-K. Then, another detector (intermediate detector) is planned to set at 2km from the target. We obtain the very similar spectrum at the intermediate detector and predict the neutrino spectrum at Super-K well.

2.6 Super Kamiokande

The Super-Kamiokande (Super-K) is used as the far detector in the K2K experiment.

The detector is the 50000 ton Water Cerenkov detector constructed under the mountain at Kamioka. Its performance and results in atmospheric neutrinos and solar neutrinos are written elsewhere [1, 3, 4].

The schematic view of the detector is shown in Fig.2.6. The detector cavity is 42m in height and 39m in diameter. There is an inner detector surrounded by an outer detector. The inner detector has 11146, 50cmϕ PMTs and the outer detector has 1885, 20cmϕ PMTs. The PMTs of the inner detector detects Cerenkov rings by relativistic charged particles which are produced by the interaction of neutrinos. The aim of the outer detector is to veto the charged particles from the outside of Super-K. The detector is very sensitive for sub-GeV neutrinos and e/μ identification, and the performance of SK is expected to be appropriate for the T2K experiment.

Interactions of neutrinos from the accelerator are identified by synchronizing the timing between the beam extraction time at the accelerator and the trigger time at

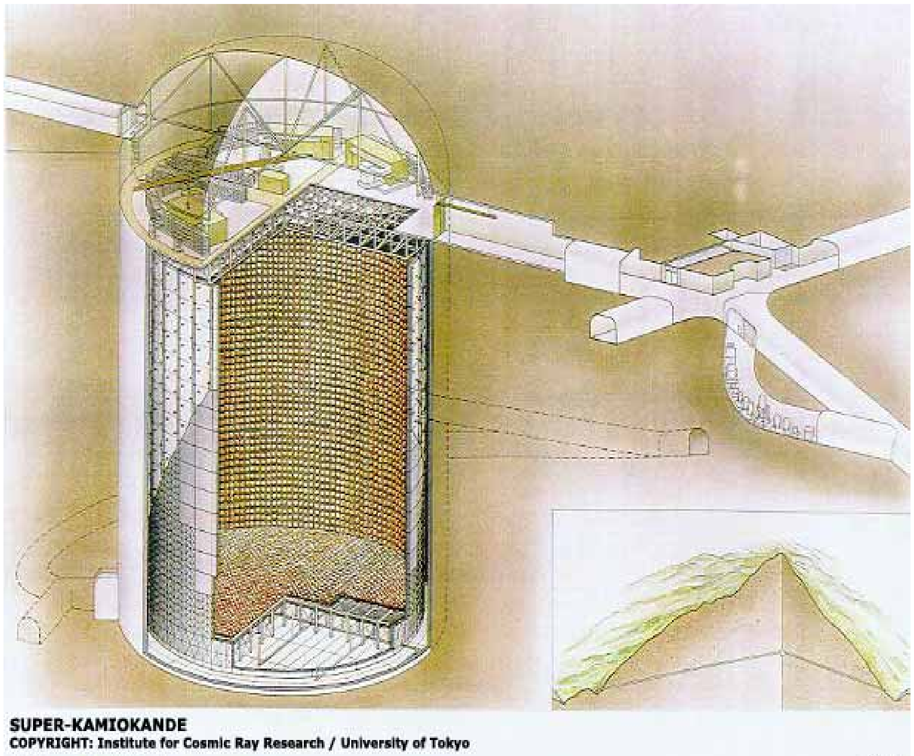

Figure 2.6: Overview of the Super-Kamiokande detector

Super-K using the GPS. The synchronization accuracy of the two sites will be less than 200ns as in the K2K experiment. The typical accidental coincidence rate of atmospheric neutrino events is much smaller than the signal rate of about $\times 10^{-3}$ / spill in the T2K experiment.

Chapter 3

J-PARC Neutrino Beamline

In this chapter, we describe the the primary proton beamline for the T2K neutrino oscillation experiment and proton beam monitors in the beamline.

3.1 Primary Proton Beamline

The primary proton beamline transports the proton beam extracted from the 50GeV PS to the target. It consists of the preparation section, the arc section and the final focusing section. The preparation section regulates the extracted proton beam to match the optics in the arc section. The arc section bends the proton beam by about 80 degrees with superconducting magnets. The final focusing section adjusts the beam size to the target size and bends the beam downward to Kamioka.

3.1.1 Preparation Section

The preparation section consists of normal conducting magnets and collimators. The aims of this section are:

- to match the beam with the suitable condition to pass through the arc section, and
- to scrape the beam halo to avoid the beam loss in the arc section.

Fig.3.1 shows the components of the preparation section and Fig.3.2 shows the designed optics parameters. The total length from the entrance to the matching point is about 55m. PHx, PVx, PDx and PQx (x is a number) indicate a horizontal steering magnet, a vertical steering magnet, a horizontal bending magnet, and a quadrupole magnet, respectively. PCx indicates a collimator between magnets.

Tables 3.1, 3.2 and 3.3 show the specification for the dipole magnets, quadrupole magnets, and collimators. The aperture of the magnets and collimators is determined to accept the beam whose emittance is 60π mm·mrad, while the emittance of the beam core is designed to be 6π mm·mrad. The beam halo whose emittance is larger than 60π mm·mrad is scraped off by collimators and magnets.

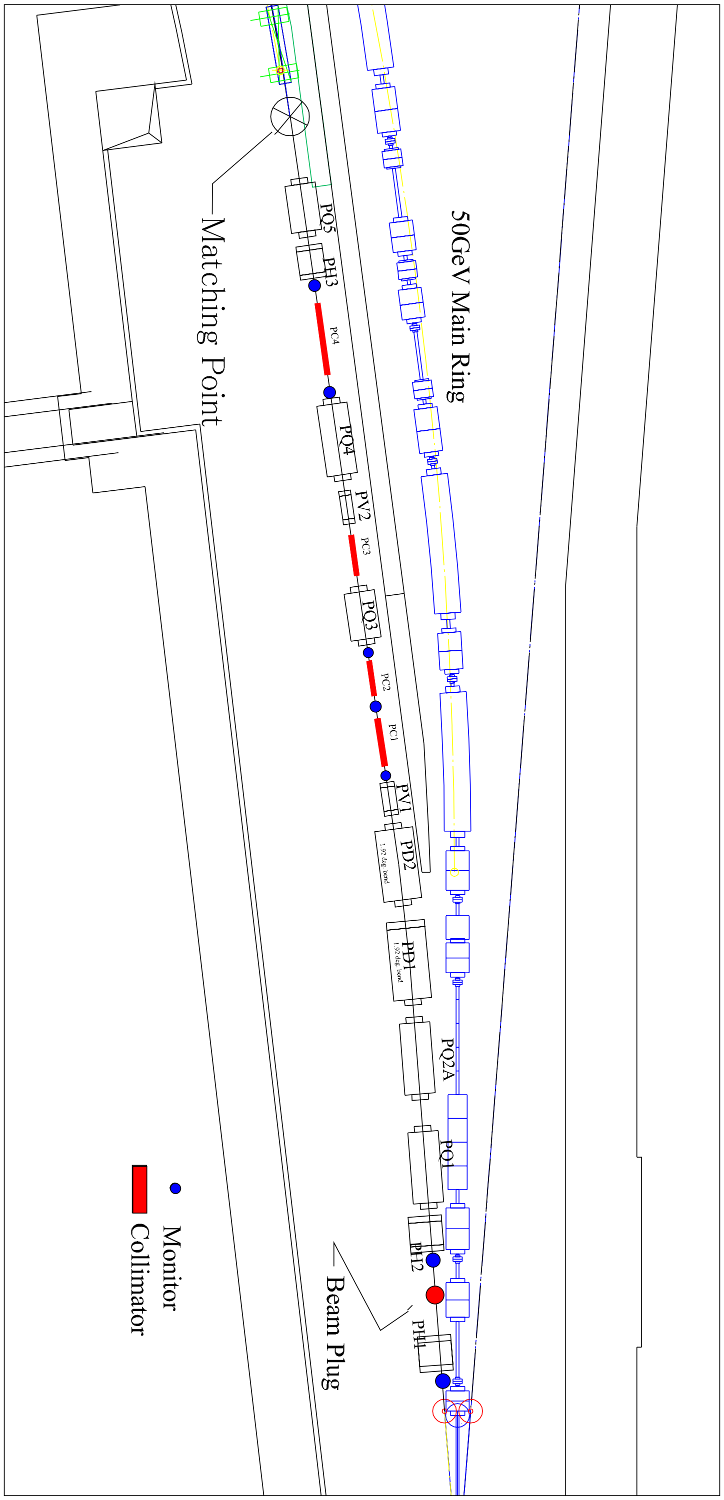

Figure 3.1: The components in the preparation section

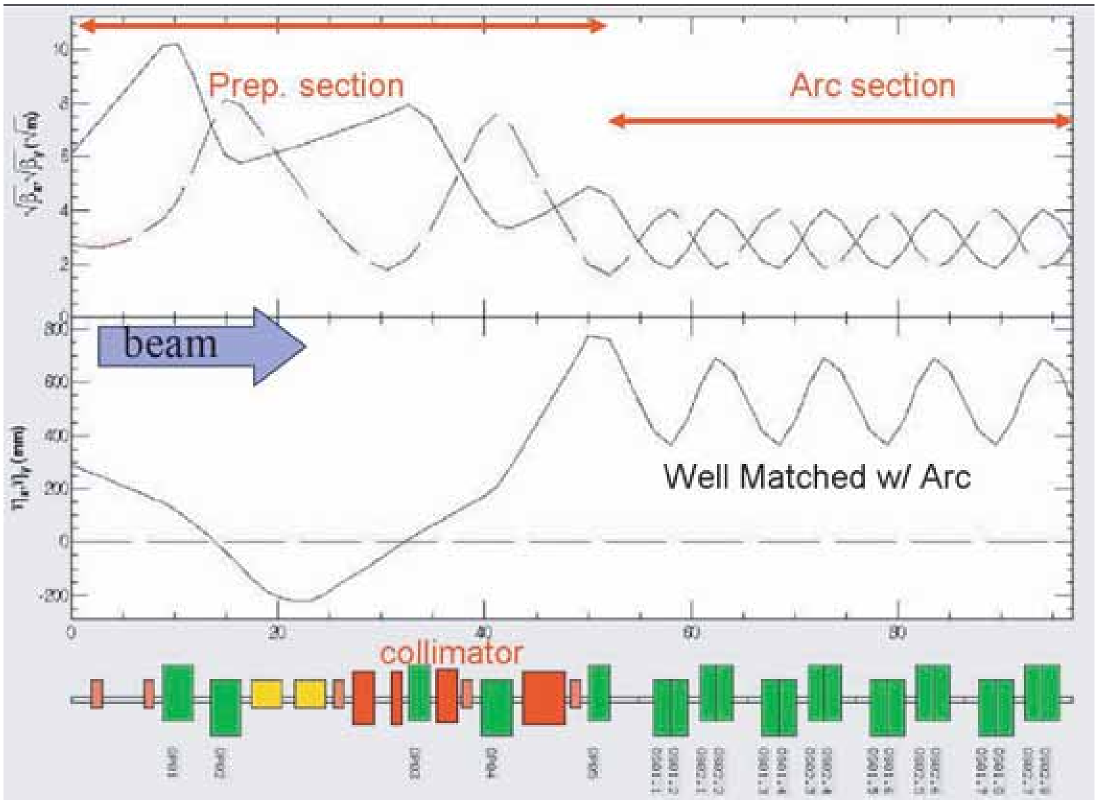

Figure 3.2: The optics calculation for the preparation section and the entrance of the arc section. The horizontal axis is length along the orbit in unit of meter. The upper graph shows the square root of β functions and the lower one shows η functions. Solid lines correspond to horizontal parameters and dashed lines correspond to vertical ones.

Name	Effective length [m]	Field strength [T]	Gap Height [mm]	Gap width[mm]
PH1	1	$0 \sim 2$	41	116
PH2	1	$0 \sim 2$	54	152
PH3	1	$0 \sim 2$	48	73
PV1	1	$0 \sim 2$	109	52
PV2	1	$0 \sim 2$	83	98
PD1	3	1.8976	115	134
PD2	3	1.8976	81	142

Table 3.1: The specification of the dipole magnets in the preparation section.

Name	Effective length [m]	Field gradient [T/m]	Aperture [mmϕ]
PQ1	3	9.1	200
PQ2	3	-11.2	150
PQ3	2	9.1	150
PQ4	3	-11.5	150
PQ5	2	15.6	100

Table 3.2: The specification of the quadrupole magnets in the preparation section.

Name	Length [m]	Gap Height [mm]	Gap width [mm]
PC1	2.0	39	115
PC2	1.45	31	121
PC3	1.7	78	109
PC4	3.0	95	64

Table 3.3: The specification of collimators in the preparation section.

3.1.2 Arc Section

The arc section consists of 28 superconducting combined function (CF) magnets. The aim of this section is to bend the proton beam by about 80 degrees toward Kamioka. The length of the arc section is about 150m, and we have to the superconducting magnets, not normal magnets. The combined function magnet has dipole and quadrupole magnetic fields in one magnet. The magnetic field expression is as follows.

$$\begin{aligned} B_x &= \pm Q \times y \\ B_y &= D \pm Q \times x, \end{aligned} \tag{3.1}$$

where D = 2.5863T is the dipole component and Q = 18.62T/m is the quadrupole field gradient.

It is the first attempt in the world to use the superconducting CF magnet in beamlines. This method has advantages. The number of magnets can be reduced comparing to the case using both dipole and quadrupole magnets. By the reduction of the number of magnets:

- We can increases the quadrupole magnets effectively and make the beam size small,
- The free spaces between magnets become wide and we can install beam monitors there, and
- The cost can be reduced.

Since the beam size is small, we can reduce the beam loss around the beamline, and effectively avoid quenching of the superconducting magnets.

Fig.3.3 shows the components of the arc section. One FODO, which consists of two CF magnets, bends the beam by 5.76 degrees. The FODO is the combination of a FOcus magnet and a DefOcus magnet. 14 FODOs are located along the beamline periodically and transport the proton beam to the final focusing section. From the beam size point of view, one FODO rotates the phase space of the beam 90 degrees. This means that the same beam optics repeats every 4 FODOs. Every 4 FODOs, we check if the beam conditions to be same, and tune the magnets.

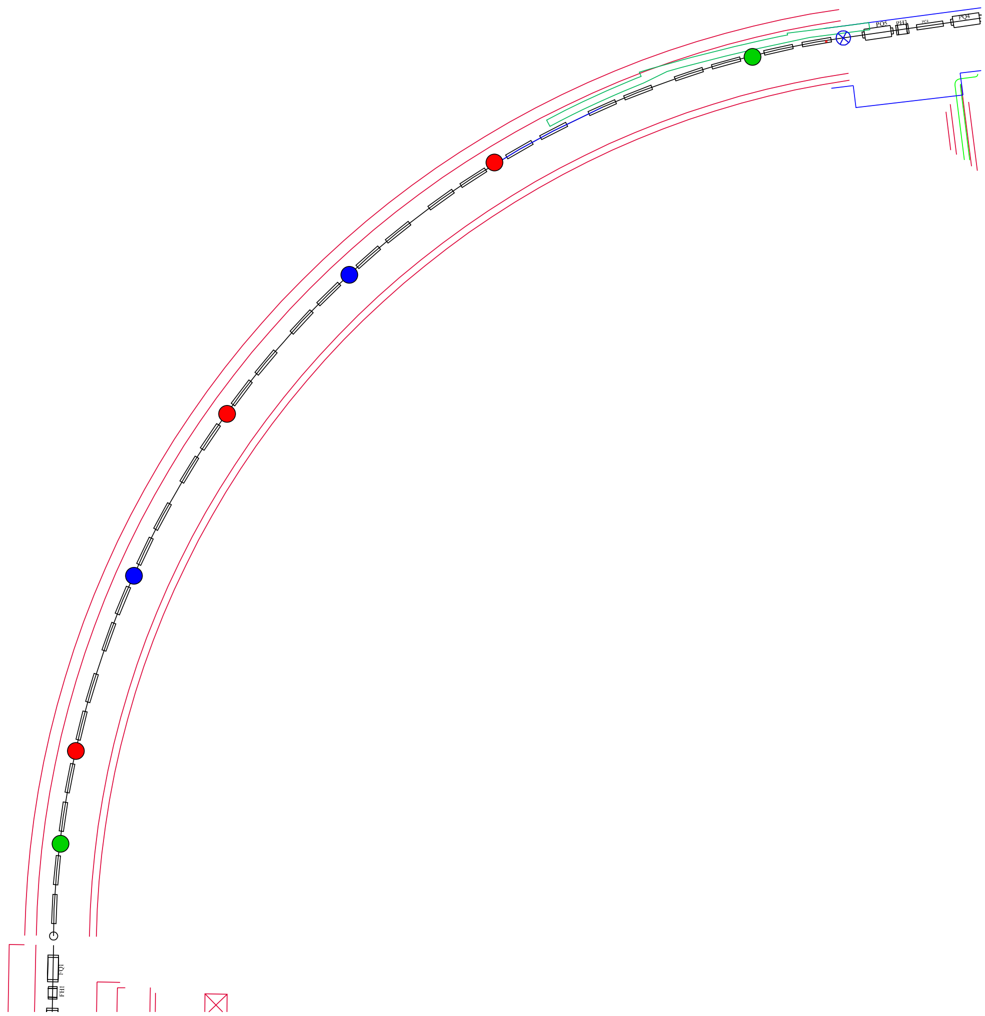

Figure 3.3: The components in the arc section. The position of the same color circles has the same optics parameters.

3.1.3 Final Focusing Section

The final focusing section consists of normal conducting magnets. The aims of this section are:

- To adjust the beam size being the target size to avoid destroying the target; and
- To bend the beam vertically to attain the Off-axis beam condition to Kamioka.

Fig.3.4 shows the components of the final focusing section and Fig.3.5 shows the designed beam optics. The length of the section is 39.4m. FHx, FVx, FVDx and FQx indicate a horizontal steering magnet, a vertical steering magnet, a vertical bending magnet and a quadrupole magnet, respectively. Tables 3.4 and 3.5 show the specification of the dipole and quadrupole magnets. We always have to assure the beam size not too small not to destroy the target. The beam at the target is deforcused to be about 30mm in diameter. The downward bending angle varies from 3.11 to 4.15 degrees, which cover the off axis angle from 2 to 3 degrees. FVD2 is used to change the off axis angle.

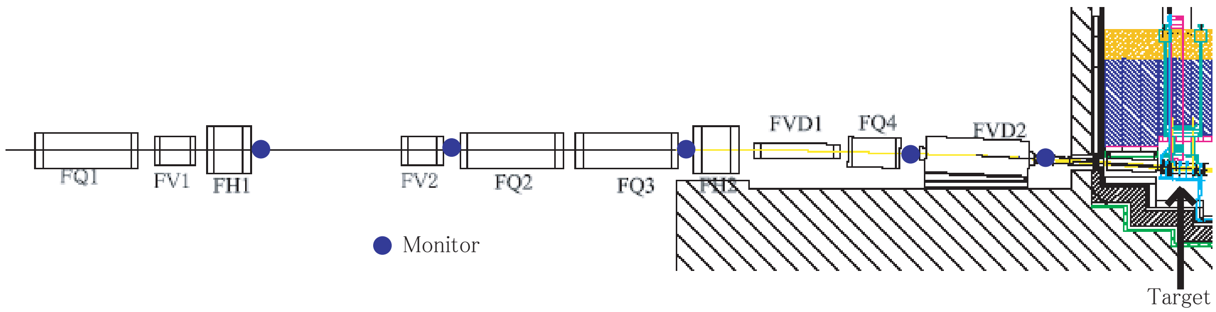

Figure 3.4: The components in the final focusing section

Name	Effective length [m]	Field strength [T]	Gap Height [mm]	Gap width[mm]
FH1	1	$0 \sim 2$	64	71
FH2	1	$0 \sim 2$	83	144
FV1	1	$0 \sim 2$	69	49
FV2	1	$0 \sim 2$	??	??
FVD1	2.5	1.896	87	162
FVD2	3.5	$1.28 \sim 2.16$	87	208

Table 3.4: The specification of the dipole magnets in the final focusing section.

Name	Effective length [m]	Field gradient [T/m]	Aperture [mmϕ]
FQ1	3	-14.3	200
FQ2	3	11.1	150
FQ3	3	-10.7	150
FQ4	1.5	2.79	150

Table 3.5: The specification of the quadrupole magnets in the final focusing section.

The aperture of the magnets is determined to accept the whole beam whose emittance is 60π mm·mrad as is the case for the preparation section.

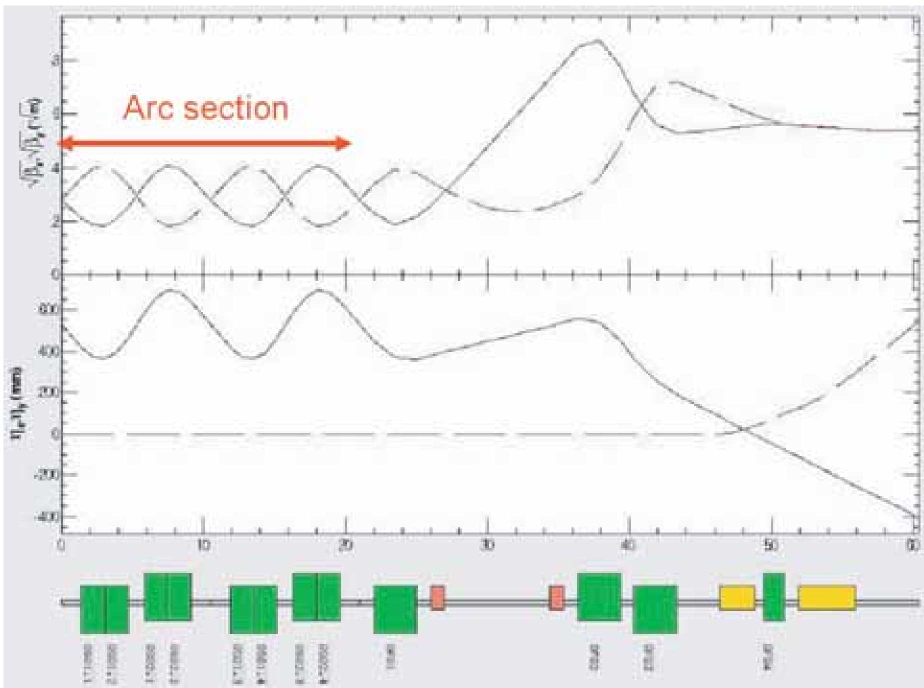

Figure 3.5: The optics of the final focusing section and the exit of the arc section. The horizontal axis is length along the orbit in unit of meter. The upper graph shows the square root of β functions and the lower one shows η functions. Solid lines correspond to horizontal parameters and dashed lines correspond to vertical ones.

3.2 Beam Monitoring System for Neutrino Beamline

To monitor and control the beam condition, the beam monitors are installed along the beamline. At present, four kinds of beam monitors listed below are considered:

- Position Monitor,
- Intensity Monitor,
- Profile Monitor, and
- Loss Monitor.

In this section, we describe the beam monitoring system at the neutrino beamline.

3.2.1 Purpose of Beam Monitors

The functions of the beam monitors are as follows. The primary function is to transport the proton beam to the target. The orbit of the beam center and the evolution of the beam size (beam optics) are calculated precisely. The real beam parameters, however, will deviate from the ideal parameters due to the finite precision for the alignment of the components, errors of the strength of the magnetic fields, non-uniformity of the magnetic fields, and so on. We, therefore, should tune all the magnets by monitoring the beam position and profile point by point to match the beam parameters to the ideal ones. The bending magnets (including steering magnets) are tuned with the beam position measured by the position monitors (and also the profile monitors). The quadrupole magnets are tuned with the beam width measured by the beam profile monitors. The combined function magnets are tuned by seeing both beam position and profile.

The second is to protect the beamline components. The high intensity beam makes an excessive radiation dose if the beam deviates from the ideal orbit. The high radiation damages all the components; especially it cause the quenching of the superconducting magnets. The amount of beam loss, therefore, must be continuously measured and the beam must must be aborted when the amount of the beam loss exceeds the limitation. For example, the limitation of the beam loss in the arc section is 1W/m. The beam loss is measured by beam loss monitors.

The third is to protect the neutrino production target. The designed target size is 3cm in diameter. The over-focused beam could destroy the target due to the excessive thermal stress.

The fourth is to measure the beam intensity. The number of protons on the target is very important information for the physics analysis.

3.2.2 Strategy of Beam Monitoring

We measure the beam center positions and profiles among the beamline components. It is desirable to install the position and profile monitors between all the components. On the other hand, since the beam monitor itself causes the beam loss and the cost reduction is necessary, the number of monitors which can be installed is limited.

Fig.3.6 shows the candidate positions of beam monitors to be installed in the beamline. The letters I, C and P indicate Intensity monitor, Center-position monitor and Profile monitor, respectively. The validity of the positions of center-position and profile monitors have been studied and described in the next chapter. The intensity monitors are installed at entrance/exit of the preparation, arc and final focusing sections. We measure energy loss at every few meters to monitor the beam loss along the beamline to avoid quenching the superconducting magnets and to protect all the components from radiation dose.

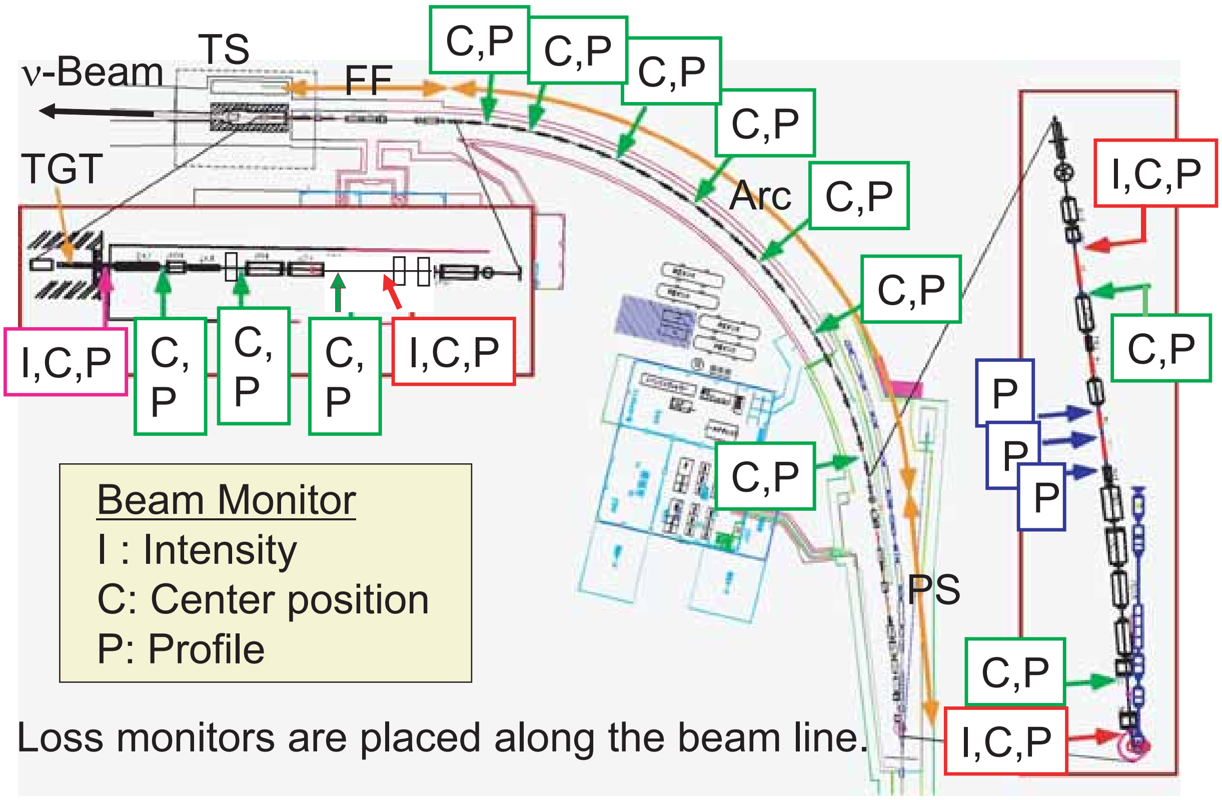

Figure 3.6: Candidate positions of beam monitors along the primary proton beamline.

The beam monitoring at the final focusing section is special, because we must always assure the beam size is not too small in order to protect the target. We have to tune the beam size at the target within an accuracy of 7%. It is necessary to measure the beam center and profile in the final focusing section continuously. There is no space in immediate proximity of the target to install a beam monitor. We have to estimate the beam size at the target by using the two beam monitors located at 4m and 8.5m away from the target.

There are other difficulties in the final focusing section. A radiation environment is too severe to access and maintain the monitors easily. The free spaces are so limited, then the size of monitors should be small enough to be installed among the beamline components.

3.2.3 Kinds of Beam Monitors

Position Monitor

As the position monitor, an Electro Static Monitor (ESM) has been developed. Four electrodes are attached on the inner wall of upper, lower, right and left side of the beam duct. The electrical potential induced by the proton beam is measured. Then, the signal asymmetries of upper and lower electrodes, and right and left electrodes are calculated, which are converted to the beam positions in the horizontal and vertical directions. The merits of the monitor are: the structure is very simple, the signal size is large, and this monitor is non-destructive. It also has the potential to provides the beam size information.

Another candidate is a Loop Pickup Monitor (LPM). The electromagnetic induction by the proton beam current is measured at the upper, lower, right and left parts. It also has the simple structure, is non-destructive type monitor, and provide a large signal.

Intensity Monitor

As the intensity monitor, a Current Transformer(CT) has been developed. The electromagnetic induction of the proton beam is measured, and the signal is in proportional to the beam intensity. This technique is already used and established in the K2K neutrino beamline. The device is also non-destructive to the beam.

Profile Monitor

As the profile monitors, we consider two types: destructive type and non-destructive type. As the destructive profile monitors, a Segmented Secondary Emission Monitor (SSEM) has been developed. Segmented thin foils made of Titanium (Ti strips) emit secondary electrons if the incident proton beam transverses these strips. Since the strips lost the negative electrons, the signal of the SSEM is positive. This technique is used in many accelerators and beamlines, and it is the primary profile monitors in the beamline. In particular, under the full intensity operation, the SSEM cannot be used because the monitor will be broken by its thermal stress and it makes a large amount of radiation loss. The SSEM is, therefore, used in the tuning time (low intensity beam), and removed from the beamline in the full intensity operation mode.

At the final focusing section, we desire other candidates of profile monitors which are non-destructive type, because it is necessary to always monitor the beam size in front of the target. As a non-destructive type monitor, Residual Gas Beam Profile Monitor (RGBPM) is the good candidate, which uses the ionization of residual gas in the beam pipe. We will describe the monitor in Chapter 5. The Halo Monitor has the same principle with SSEM but the center part is removed. By measuring the beam halo around the beam core, we estimate the beam size. This is also a kind of non-destructive because it does not interrupt the beam core.

Loss Monitor

As the Beam Loss Monitor (BLM), an ion chamber has been developed. High voltage is applied to the coaxial metal tube into which air is poured, and the air ionized by the charged particles is collected and read out. The signal is proportional to the beam loss. BLM will be installed around the beam duct every few meters along the beamline.

Chapter 4

Study of Beam Monitoring Scheme at Primary Proton Beamline

In the J-PARC neutrino beamline, it is important to control the proton beam precisely as described in the previous chapters. Not only at the beginning of the experiment but during the whole operation time of the experiment, we must periodically tune the magnets and confirm that the proton beam is correctly delivered to the target.

The beam tuning is performed as follows:

1. Tune the bending and steering magnets so that the beam passes through the center of the beamline;
2. Measure the beam emittance and twiss parameters; and
3. Tune the quadrupole magnets to match the beam width with the designed beam optics.

Position and profile monitors are used for the tuning. We should check if the number and the positions of beam monitors to be installed are appropriate to tune the beam precisely. We consider the positions and the number of steering magnets. To check them, we perform beamline simulations. In the following sections, we describe the tuning of the beam center and the measurement of the beam emittance at the preparation section.

4.1 Monte Carlo Simulation with Geant4

In this study, Geant4 package[7] is used to simulate the proton beam delivery. Along the beamline, we put magnets, beam ducts and collimators according to the beam optics design. Initial protons are injected from the extraction point of the 50GeV accelerator. Their trajectories at the position of each component are calculated along the beamline. In the simulation code, the magnetic fields are applied as is designed [6]. However all the components consist of air (protons do not interact the components), to speed up the calculation speed. To estimate the amount of the beam loss, the number of protons which hit the components is counted.

In Table 4.1, we describe the beam core parameters at the extraction point used in the simulations. These values are reported by the 50GeV accelerator group [6].

Beam Energy	50[GeV]
Beam Emittance	6π[mm·mrad]
(β_x, β_y)	(37.207 , 7.398)m
(α_x, α_y)	(-2.731 , 0.306)
(η_x, η'_x)	(0.290 , -0.016)
(η_y, η'_y)	(0.0 , 0.0)
Momentum dispersion	0.3%

Table 4.1: Parameters of the primary proton beam extracted from the 50GeV accelerator.

The distribution of the extracted beam is assumed to be flat in the emittance ellipse whose area is 6π mm· mrad. The distributions in the phase space and the profiles in the real space of the beam at the entrance of the beamline are shown in Fig.4.1. X and Y are defined as the horizontal and the vertical direction, respectively. The beam size at each component is defined as 2× RMS of the beam profile. (See Appendix B.1.) We do not take into account of the beam halo in this study.

4.2 Beam Monitoring and Tuning Scheme at the Preparation Section

In this section, we describe the tuning of the beam center in the preparation section. Considering the resolution of the beam monitor and the precision of the alignment, the accuracy of the beam position measurement is assumed to be 0.5mm. We assume that all the monitors along the beamline have the same accuracy. Fig.4.2 schematically shows the components in the preparation section.

4.2.1 Tuning the beam center in the X direction

The deviation in the beam position between the ideal value and the real value in the X direction comes from the following two sources: the deviations in the incident beam parameters from the accelerator, and the error of the magnetic field strength of the bending magnets, PD1 and PD2. We study the tuning scheme to recover these deviations.

Correction of the deviation in the incident beam center

Since the incident beam is extracted with the kicker magnet of the accelerator, the beam center in the X direction is influenced by the error of the kicker magnet. The uncertainty of the incident beam is at most ±18mm in the center position or ±1mrad in the incident angle without an accelerator tuning. With the accelerator tuning, the uncertainty is estimated about to be ±2mm or ±0.2mrad. In the simulation, we assumed a larger deviation, 10mm or 1mrad. Fig.4.3 shows the evolution of the deviation from the design orbit caused by the incident beam position movement of 10mm or the incident beam direction deviating 1mrad. If we do not tune the beam using the steering magnets, the deviations in the beam center at the exit of the preparation section become (-19.0mm,

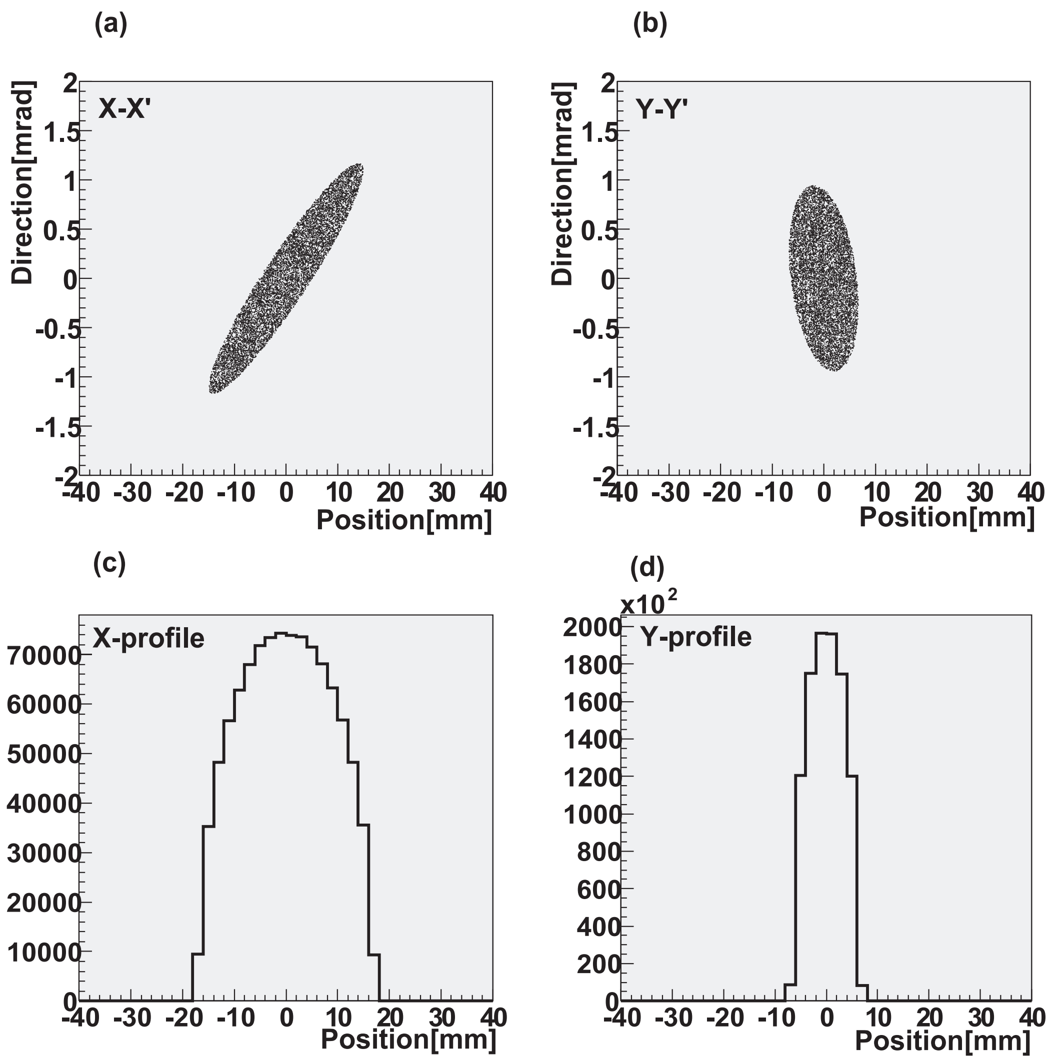

Figure 4.1: Phase spaces of the extracted proton beam in (a) X-X' and (b) Y-Y', and beam profiles (c) in the X direction and (d) in the Y direction.

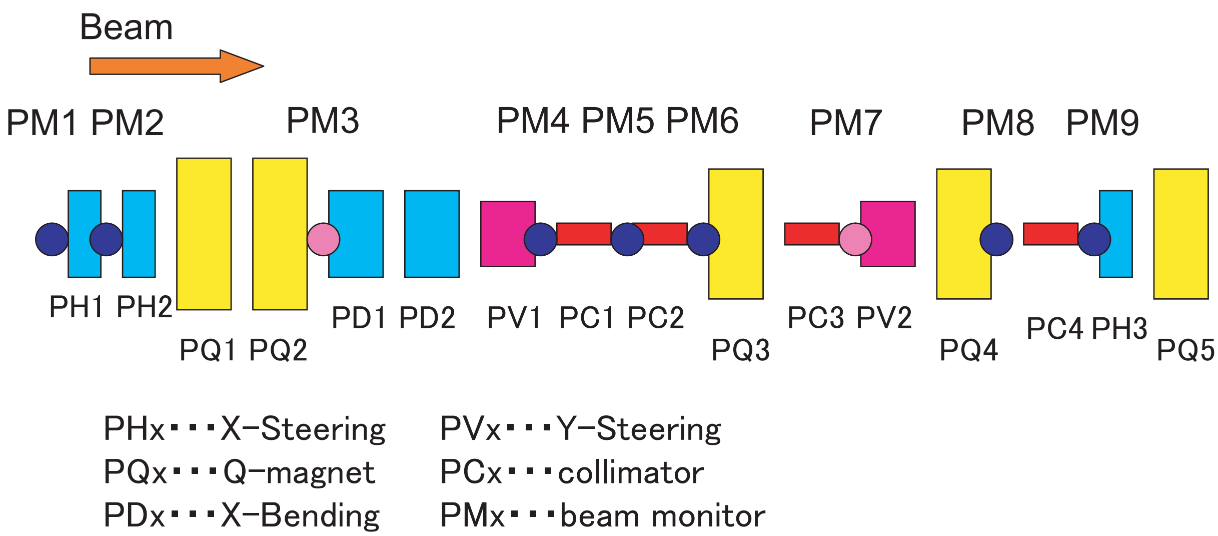

Figure 4.2: Schematic view of the components in the preparation section. Blue circles are the positions of beam monitors to be installed and pink circles are the introduced positions of beam monitors in our study. The length of each component and the distance between nearby components are arbitrary.

and -1.5mrad) and (25.5mm, and 1.5mrad), for 10mm movement and 1mrad deviation, respectively,

These deviations are corrected using the steering magnets, PH1 and PH2. They are the first two steering magnets in the beamline. Fig.4.4 shows the outline of the tuning scheme. The tuning scheme is as follows:

1. Control the beam center to pass through the center of the PH2 magnet using the PH1 magnet, and
2. Correct the beam direction using the PH2 magnet.

In general, two steering magnets can modify any off beam. For example in the case that the incident beam shifts by 10mm at the entrance, the beam is corrected with the PH1 magnetic field of -0.34T and the PH2 magnetic field of 0.34T. In the case that the incident beam is bent by 1mrad at the entrance, the beam is corrected with the PH1 magnetic field of -0.23T and the PH2 magnetic field of 0.08T.

With the current proposed monitor positions, however, we cannot verify the tuning with PH2 is correct because there is no monitor between PH2 and the downstream bending magnets. Therefore we have to put another monitor there. The additional monitor, PM3 is decided to be installed just before the PD1 magnet to improve the beam position resolution at PD1. We define the beam position accuracy as the maximum deviation if orbit of the beam randomly deviates within 0.5mm at the beam monitors. Considering the resolution of the monitor, the beam position accuracy at PD1 is about 0.7mm. The remained error is corrected simultaneously in the tuning of the magnetic field strength of PD1 and PD2.

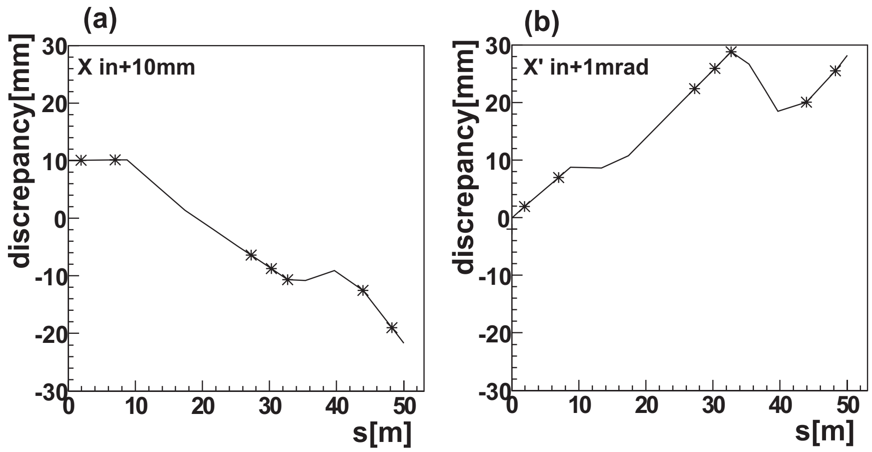

Figure 4.3: Evolution of the beam position deviation from the designed orbit if (a) the extracted beam shifts 10mm and (b) the extracted beam is bent 1mrad. The horizontal axis means the distance along the beamline in the X direction. The marks (*) indicate the positions where monitors are installed.

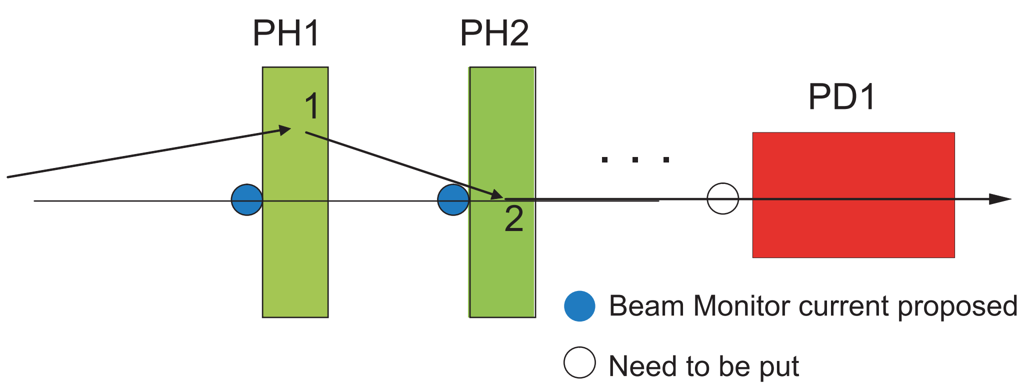

Figure 4.4: Outline of the tuning scheme with PH1 and PH2.

Correction of the errors of the bending magnets' strength

Fig.4.5 shows the deviations in the beam center positions caused by the errors in the magnetic fields of PD1 and PD2. These deviations are recognized by the three monitors: PM4, PM5 and PM6 around the PC1 and PC2 collimators. One can see in Fig.4.5 (c), the beam center shifts parallel to the designed orbit if the magnetic fields of PD1 and PD2 have positive and negative errors, respectively. We use this effect for the beam tuning.

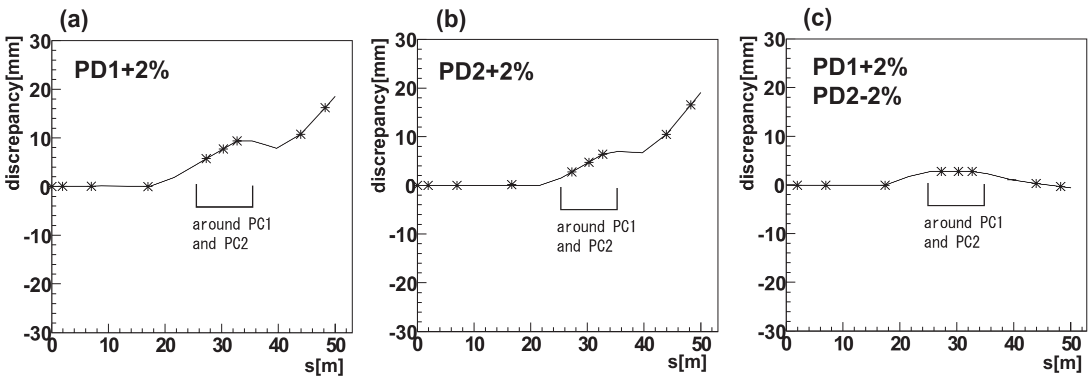

Figure 4.5: Evolution of the beam position deviation from the design orbit if (a) the magnetic field of PD1 is increased by 2% , (b) the magnetic field of PD2 is increased by 2% and (c) the magnetic field of PD1 is increased by 2% and that of PD2 is decreased by 2% .

Fig.4.6 shows the outline of the tuning scheme. The scheme is as follows:

1. Control the beam to be parallel with the designed orbit at PM4, PM5 and PM6 around PC1 and PC2, changing the magnetic field of PD1 (or PD2), and

2. Control the beam center to pass through the designed orbit changing the magnetic fields of PD1 and PD2 simultaneously and inversely.

However, these three monitors do not have sufficient resolution to tune the PD1 and PD2 magnets based on this method. The accuracy of the beam position at the exit of the preparation section is over 4mm if we tune the dipole magnets using only the three monitors. We, therefore, should also use the downstream monitors in the tuning of PD1 and PD2. By using PM4, PM5, PM6 and PM9, the accuracy of the tuning becomes the same order as the resolution of the beam monitor.

4.2.2 Tuning the beam center in the Y direction

The deviation from the design orbit in the Y direction comes from the following two reasons: the deviation in the incident beam from the accelerator, and the inclination of the bending magnets, PD1 and PD2. We study the tuning scheme to correct these deviations.

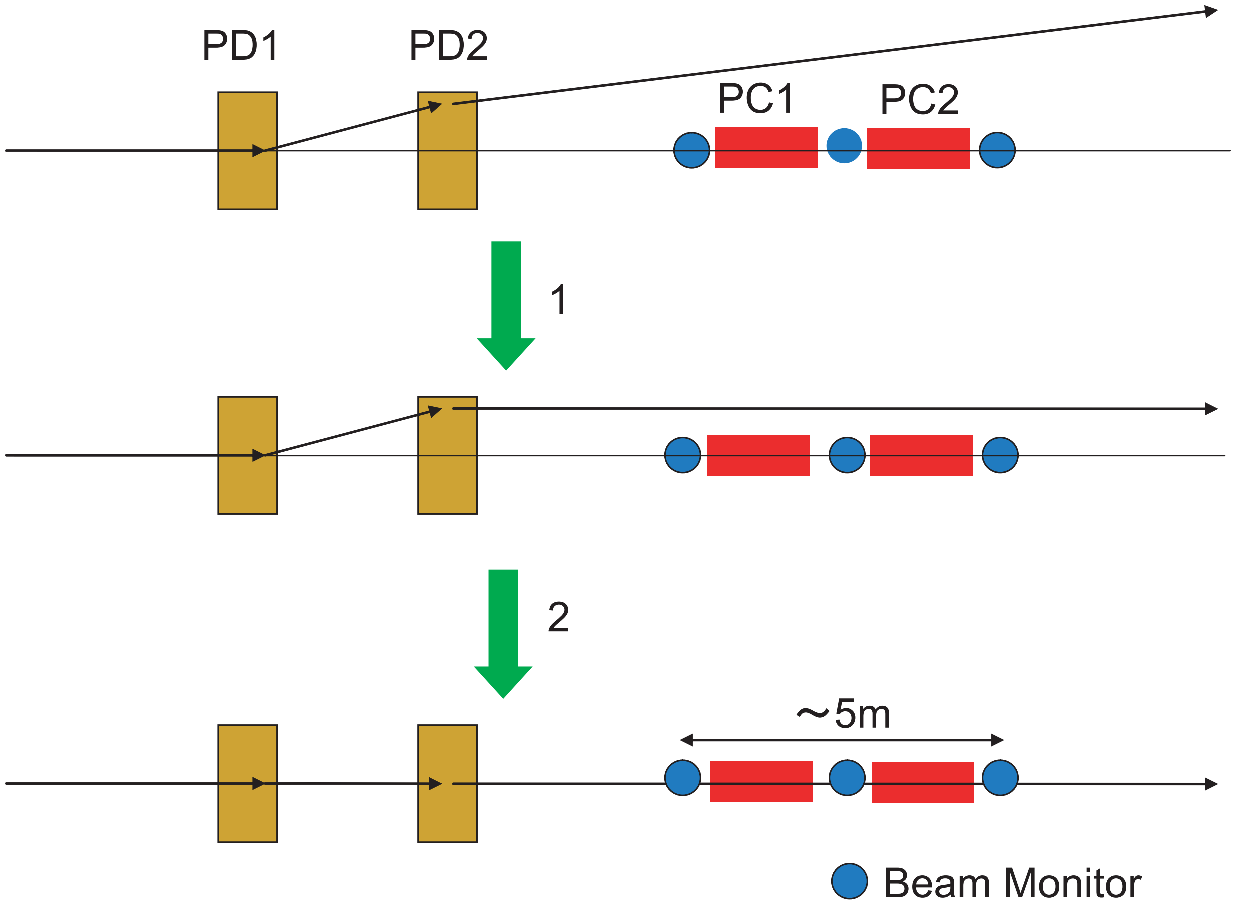

Figure 4.6: Outline of the tuning scheme of PD1 and PD2.

Correction of the deviation in the incident beam position

Fig.4.7 shows the evolution of the deviation from the design orbit in the Y direction, caused by the incident beam center movement of 10mm or the incident beam direction deviating 1mrad. At the exit of the preparation section, the deviations in the beam center become (-4.5mm , 2.6mrad) and (-5.5mm, 1.0mrad), in the cases of 10mm moving and 1mrad deviation, respectively. We expect that the deviation in the incident beam center in the Y direction is small than the current assumption, since the accelerator and the beamline are on the same plane.

The tuning of these deviations is carried out using the vertical steering magnets, PV1 and PV2. The tuning process is almost the common as that in the X direction. First, we control the beam to go through the center of the PV2 magnet, and then control the beam to go straight with the PV2 magnet. In the first step, we need another beam monitor to measure the beam center position at the PV2. Considering the free space, we decide to put a new monitor just before the PV2 magnet. For example in the case that the incident beam shifts 10mm, the beam position is corrected with the PV1 magnetic field of 0.22T and the PV2 magnetic field of 0.02T. In the case that the incident beam is bent 1mrad, the beam center is corrected with the PV1 magnetic field of 0.10T and the PV2 magnetic field of 0.09T. The precision of the beam center at the exit of the preparation section is estimated to be about 1mm or 0.1mrad.

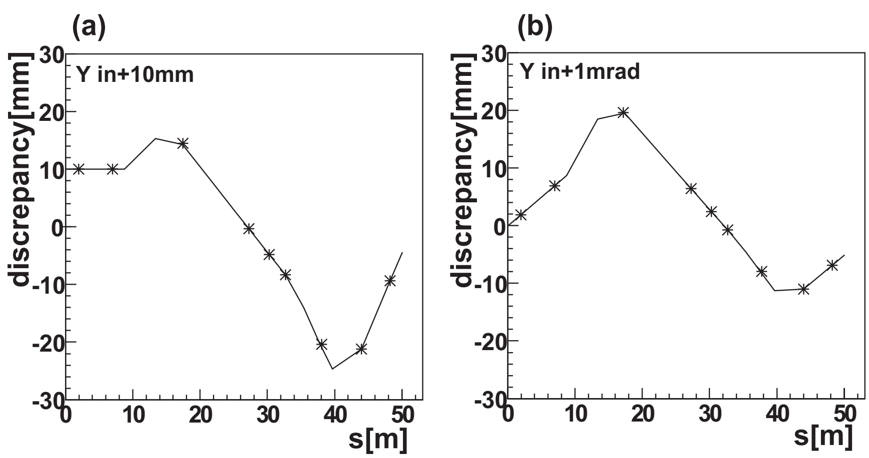

Figure 4.7: Evolution of the beam position deviation from the design orbit if (a) the extracted beam shifts 10mm and (b) the extracted beam is bent 1mrad in the Y direction.

Correction of the error caused by the inclination of bending magnets

The misalignment of the horizontal bending magnets causes a beam center deviation in the vertical direction. We study the case that the bending magnet is rotated around the beam axis. Fig.4.8 shows the beam position deviation if the PD1 magnet is rotated at 5mrad around the beam axis. For the X direction, the decrease of the magnetic field is negligible. Such a deviation can be corrected by the vertical steering magnets, PV1 and PV2, since the steering magnets are located downstream of the PD1 and PD2. The alignment accuracy expected to be much smaller than the assumption of this study, and the tuning is possible.

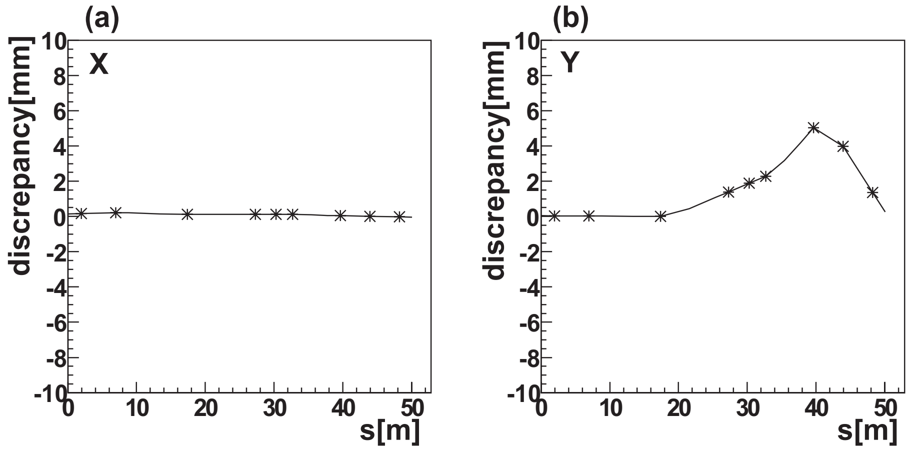

Figure 4.8: Evolution of the beam position deviation (a) in the X direction and (b) in the Y direction from the design orbit if the PD1 magnet is rotated at 5mrad around the beam axis.

4.3 Beam Monitoring Scheme at the Arc Section

In this section, we describe the deviation from the design orbit in the arc section. Fig.4.9 schematically shows the components in the arc section.

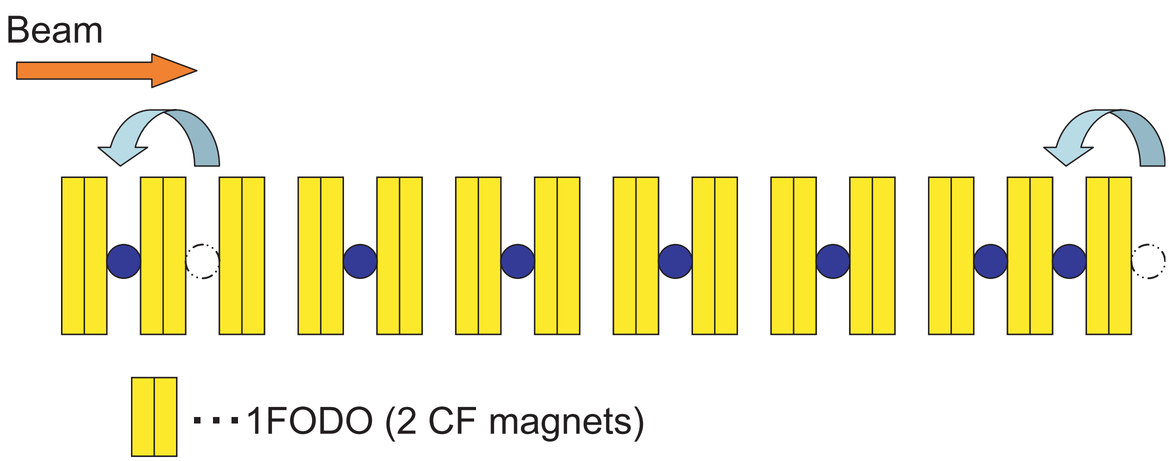

Figure 4.9: Schematic view of the components in the arc section. The number of FODOs is 14. Blue circles are the positions of beam monitors to be installed. The length of each component and the distance between nearby components are arbitrary.

In the arc section, the phase space of the beam has a periodic evolution for eight superconducting magnets, which correspond to four FODO cells. The monitors are located every two FODO cells. The first and the final monitor are moved for one cell from this basic position as shown in Fig4.9. We can, therefore, measure the profile every FODO cell, if the periodic evolution of the beam optics is assumed. The tuning at the arc section is carried out by confirming that the beam profiles at every four FODOs are identical. Fig.4.10 shows the evolution of the beam position deviation for the four FODO cells. We assumed the deviation at the exit of the preparation section is 1mm or 0.1mrad based on the obtained results from the preparation studies.

We find the amount of the deviation is the same at the entrance and the exit of the four FODO cells. The deviation after the second FODO has the inverse sign of the entrance deviation. This is consistent with the fact that the phase space of protons has rotated by 180 degrees with respect to the entrance. The maximum deviation in the beam center position is about 2mm, which is small enough from the point of the beam loss.

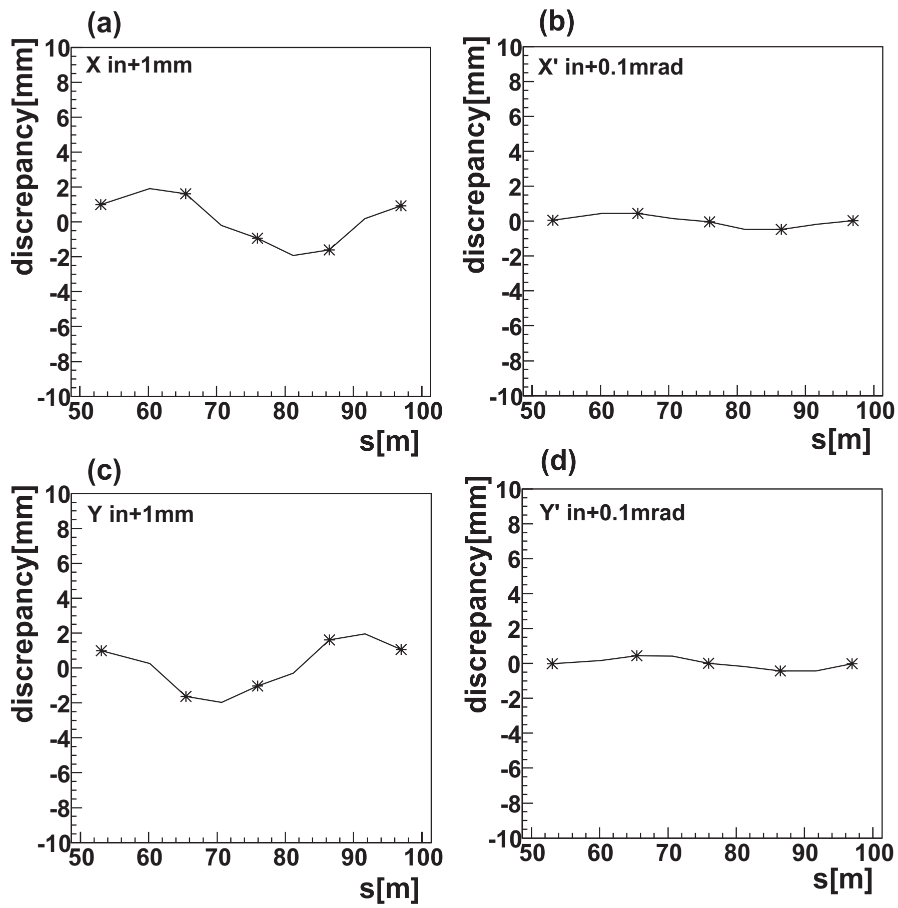

Figure 4.10: Evolution of the beam position deviation from the design orbit in four FODO cells for the cases: (a) The beam is shifted 1mm in the X direction at the entrance; (b) The beam is shifted 0.1mrad in the X direction at the entrance; (c) The beam is shifted 1mm in the Y direction at the entrance; and (d) The beam is shifted 0.1mrad in the Y direction at the entrance.

4.4 Beam Monitoring and Tuning Scheme at the Final Focusing Section

In this section, we describe the beam position tuning at the final focusing section. Here the beam center deviation is caused by 1) the propagation of the deviations in the preparation section and the arc section, and 2) the uncertainty of the magnetic fields of the vertical bending magnets, FVD1 and FVD2. The final vertical bending has a direct impact on the off-axis angle of the neutrino beam, and a deviated beam can easily destroy the target if the beam position is different from the designed value. For the reasons, the correct tuning of FVD1 and FVD2 is especially important. Fig.4.11 schematically shows the components in the final focusing section.

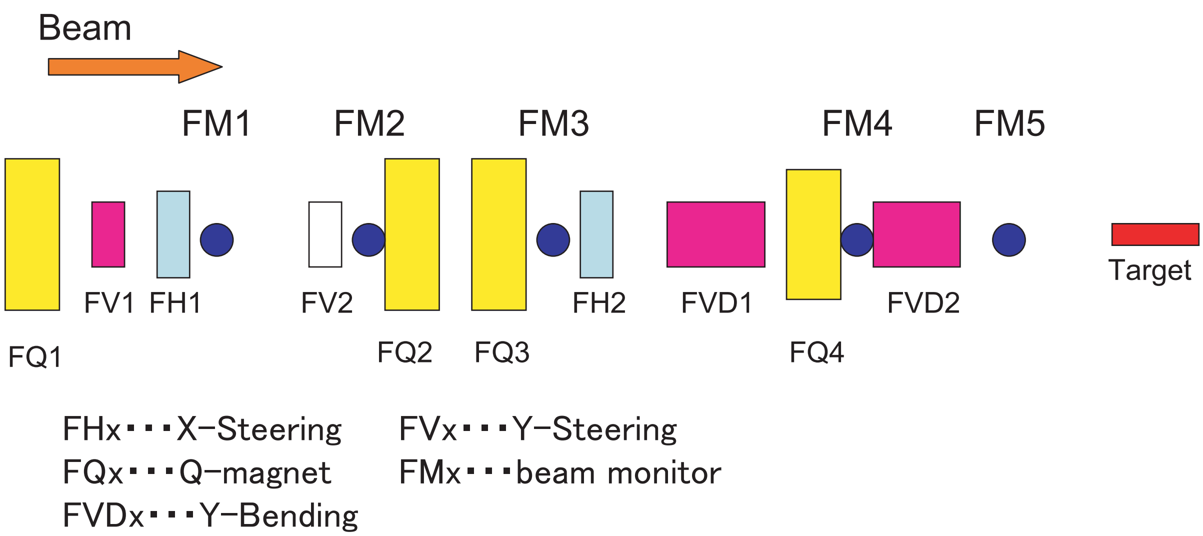

Figure 4.11: Schematic view of the components in the final focusing section. Blue circles are the positions of beam monitors to be installed. FV2 is the magnet which we introduce in this study. The length of each component and the distance between nearby components are arbitrary.

4.4.1 Tuning the beam center in the X direction

The deviation in the beam center is caused only by the deviation of the beam in the arc section. Fig.4.12 shows the deviations in the beam center position at each component caused by the deviation of the beam center position and the beam direction of 1mm and 0.1mrad, respectively. These values are the same as those in the arc section studies. Around the second monitor, the beam deviation is 5mm at maximum. Since the quadrupole magnet FQ1 acts as a defocus magnet in the X direction, the deviation is enhanced after FQ1.

The deviation can be corrected with the steering magnets, FH1 and FH2. The method is the same as in the preparation section. We control the beam to go straight with the

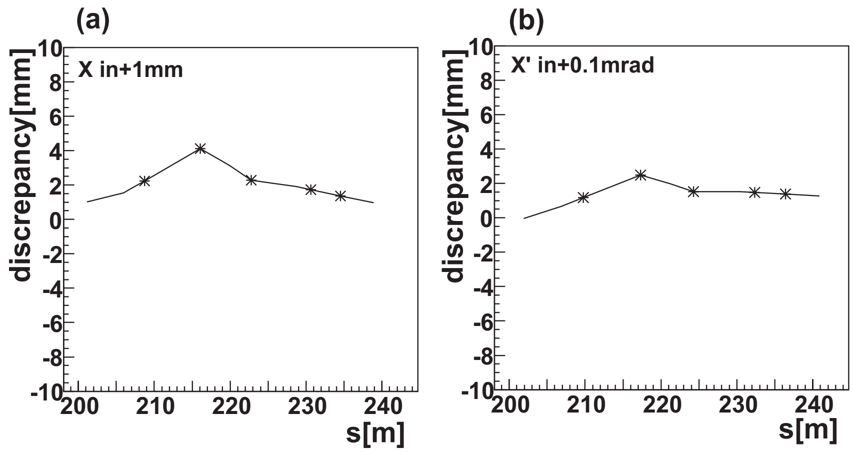

Figure 4.12: Evolution of the beam position deviation from the design orbit in the final focusing section for the cases if (a) the extracted beam shifts 1mm, and (b) the extracted beam is bent 0.1mrad.

FH2 magnet. In the case that the incident beam is shifted by 1mm, the beam is corrected with the FH1 magnetic field of 0.05T and the FH2 magnetic field of -0.05T.

The position accuracy at the target in the X direction is determined by the tuning accuracy of the FH2 magnet. Considering the resolution of the final monitor, the position accuracy at the target is estimated to be about 0.8mm. This is good enough to protect the target and to tune the off-axis angle of the neutrino beam. It is not necessary to add another steering magnet or beam monitor for the tuning in the X direction.

4.4.2 Tuning the beam center in the Y direction

Fig.4.13 shows the deviation in the beam center position in the Y direction at each component. They are caused by the deviation of the beam center position of 1mm and the beam incident angle of 0.1mrad at the entrance of the final focusing section, respectively. Around the third monitor, the beam deviation is 5mm at maximum. Since the quadrupole magnet FQ2 acts as a defocus magnet in the Y direction, the deviation is enhanced after FQ2.

We need at least two steering magnets to correct the beam deviation, although there is one steering magnet (FV1) on the present design. In principle, we can correct these deviation using the vertical bending magnets FVD1 and FVD2. However, the accuracy of the beam position measurement at the center of the FVD1 magnet is worse, and it makes the accuracy of the position at the target worse.

Without FV2, we consider the following tuning scheme. The beam is tuned to pass the center of FVD1 with FV1. To measure the beam position at the center of FVD1, we have to know the direction of the beam after the FQ3 magnet. We introduce another monitor just before FVD1 to measure the beam direction with the new monitor and the FM3 monitor. The accuracy of the beam position at the center of FVD1 is, however, 1.4mm since the lever arm between the two monitors is short.

On the other hand, with the FV2 magnet, we can tune the beam position and direc-

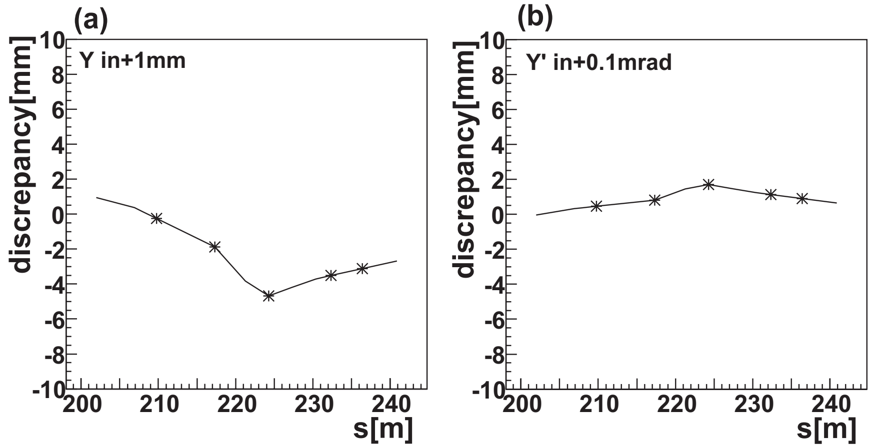

Figure 4.13: Evolution of the beam position deviation from the design orbit in the final focusing section for the cases if (a) the extracted beam shifts 1mm, and (b) the extracted beam is bent 0.1mrad.

tion before the FQ2 magnet using two steering magnets, FV1 and FV2. The beam is not so much bent by FQ2 and FQ3 if the beam pass through the center of these magnets. By measuring the beam positions at FM2 and FM3, the beam position at the center of FVD1 can be measured. The accuracy of the measurement is about 0.5mm. Here after, we assume the FV2 is installed in the beamline to improve the accuracy. Then we include the FV2 in our studies. In the case that the incident beam is shifted 1mm, the beam position is corrected with the FV1 magnetic field of 0.03T and the FV2 magnetic field of 0.01T.

In the next step, we tune the FVD1 magnet. We control the magnet by measuring the beam center position at the FM4 monitor in front of the FVD2 magnet. Although there is a quadrupole magnet between the FVD1 and the monitor. we can regard it as a drift space since the magnetic field is weak and the length of the magnet is short. In the worst case, the beam position at FVD1 deviates 0.5mm and the measured beam center at FM4 deviates -0.5mm. In this case, the beam position at the center of FVD2 can be measured with an accuracy of 1.1mm.

In the final step, we tune the FVD2 magnet using the final beam monitor, FM5. The accuracy of the beam position measurement at the target is calculated to be 2.8mm in the similar way of the tuning of FVD1, although we need 1mm accuracy to protect the target. The significant distance between the monitor and the target leads to the poor position accuracy at the target. Fig.4.14 shows the calculated position accuracy in the Y direction at the target as a function of the distance between the final beam monitor and the target. To achieve the 1mm accuracy, the final monitor should be installed within 1.5m from the target, which is hard from the limitation of the space. We need the rearrangement of some beamline components around the target and/or the development of the special monitor to improve the resolution of the beam position measurement.

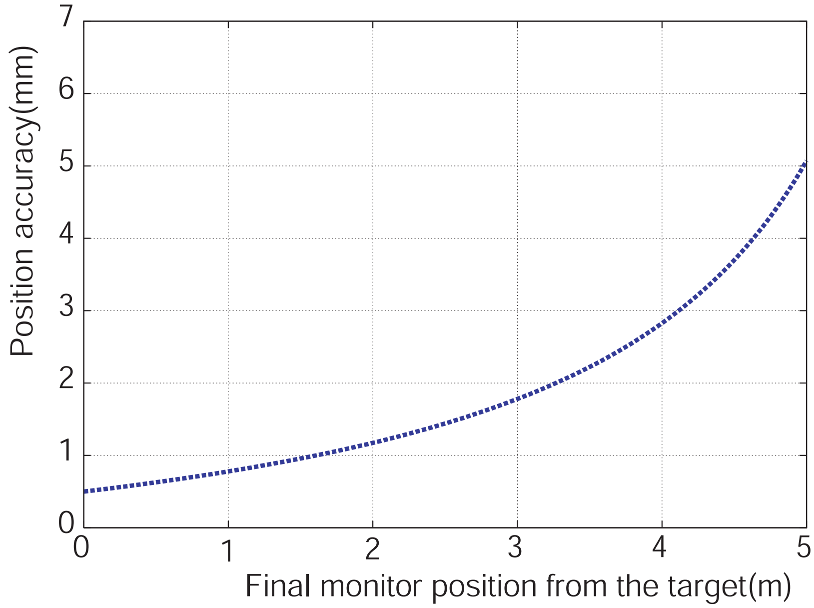

Figure 4.14: Relation between the position of the final profile monitor from the target and the position accuracy at the target.

4.5 Beam Emittance Measurement at the Preparation Section

In this section, we describe the emittance measurement at the preparation section. The emittance of the beam core is expected to be 6π[mm·mrad] based on the the accelerator group report[6]. After extracting the beam to the neutrino beamline, we need to measure the emittance. The measured emittance is used for the tuning of the quadrupole magnets, and for the estimation of the beam size at the target. We require the emittance measurement within a 10% accuracy.

The beam emittance is related to the beam size. The emittance is calculated from the information of the beam profile monitors. Other parameters related to the beam size are twiss parameters, α, β, γ (See Appendix B). Here the emittance is one of the beam parameters, and is conserved after extracting the beam. The twiss parameters are the parameters which are determined by the beamline components. The set of the three parameters: α, β, γ has two degrees of freedom. The beam size is determined by the three degrees of freedom: one from the emittance and two from the twiss parameters. The emittance measurement, therefore, needs beam size measurements with more than three different monitors or with more than three different quadrupole magnetic field.

There are three methods to measure the beam emittance:

1. To use beam monitors in the drift space [9] (Method 1),

2. To measure the beam size changing with various quadrupole magnetic field[9, 10] (Method 2), and

3. To use all the monitor information including quadrupole magnet errors (Method

3).

We study the error and feasibility of the emittance measurement of each method. We ignore the energy dispersion here, and calculate its effect later.

Resolution of the profile measurement

First, we estimate the resolution of the profile measurement. In the beam tuning, SSEM is used as a profile monitor. The strips of SSEM, whose width is 1mm, are spaced on 2mm center. The sources of systematic errors are the electric noise, the gain calibration of each anode (or aging), the alignment of the strip positions and the monitor itself, and so on. According to a reference [8], the measured resolution of the 1σ beam size is about 0.17mm with the strip pitch of 1mm assuming the distribution of the beam is a Gaussian function. The beam size in the reference is almost the same as our beam size.

We assume that the resolution of the beam size is proportional to the strip pitch. In our definition of the beam size to be $2 \times RMS$, the resolution of SSEM is assumed to be 0.7mm. In the following study, we assume this value as a resolution of the profile monitors. Since the systematic error of our SSEM is not the same as that in the reference, the other measurements on the systematic errors of our SSEM is necessary for the future studies.

Method1

Method 1 uses four monitors along the drift space between PQ2 and PQ3. Though the sections of the bending magnet PD1 and PD2 are not drift spaces, the focusing part of the transfer matrices of PD1 and PD2 are so small that we can ignore them. The advantage of this method is to measure the emittance without the error of quadrupole magnets. The disadvantage is that the accuracy of the measurement is not so good since the number of monitors is limited.

Along the drift space, the square of the beam size (w^2) is expressed as a parabolic function of the orbit length s. The function is

$$w^2 = \epsilon\beta - 2s\epsilon\alpha + s^2\epsilon\gamma, \tag{4.1}$$

where the twiss parameters are for the first monitor, and s is the distance from the first monitor to each monitor. The result of fitting the squared beam sizes with the function is shown in Fig.4.15. The calculated emittance is

$$\begin{aligned} \epsilon_x &= 6\pi \pm 13\pi \\ \epsilon_y &= 6\pi \pm 0.67\pi. \end{aligned}$$

The emittance center value is correctly calculated to be 6π , but the error is much more than 10% in the X direction. The error in the Y direction is relatively small since the variation of the β function is large.

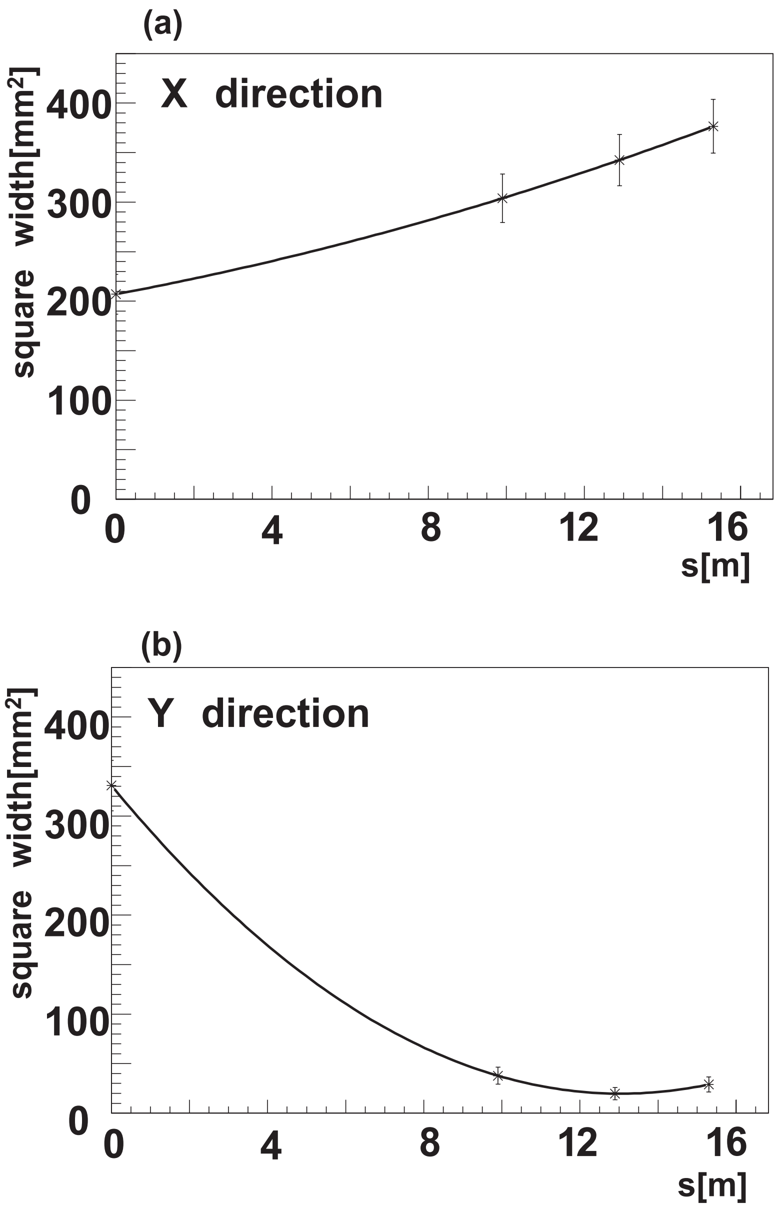

Figure 4.15: Beam size evolution in the drift space of the preparation section in (a) the X direction and (b) the Y direction. The horizontal axis is the orbit length from the first monitor and the vertical one is the squared beam size. These plots are fitted by a parabolic function.

Method2

Method 2 is to measure the variation of the beam size as changing the upstream quadrupole magnet. In our study, we change the PQ2 magnetic field and measure the beam size at the PM4 monitor before PC1. The advantage of this method is that it is usually adopted and established at a lot of accelerators and beamlines. The disadvantage is that it may cause hard radiation damage in the downstream section since the beam optics is deviated from the designed optics.

We define $\alpha_0, \beta_0, \gamma_0$ as the twiss parameters just before the PQ2 magnet, and the transfer matrix to the monitor as M. The matrix M is a function of the magnetic field of PQ2. The beam parameters at the measuring monitor are expressed as

$$\begin{pmatrix} \epsilon\beta & -\epsilon\alpha \\ -\epsilon\alpha & \epsilon\gamma \end{pmatrix} = M \begin{pmatrix} \epsilon\beta_0 & -\epsilon\alpha_0 \\ -\epsilon\alpha_0 & \epsilon\gamma_0 \end{pmatrix} M^T, \tag{4.2}$$

where $\epsilon\beta$ is the squared beam size. By varying the PQ2 magnetic field, that means, changing the transfer matrix M, we measure the beam sizes at PM4. Then we can calculate the emittance.

Fig.4.16 shows the fitting result. The calculated emittance is

$$\begin{aligned} \epsilon_x &= 6\pi \pm 0.42\pi \\ \epsilon_y &= 6\pi \pm 3.6\pi. \end{aligned}$$

We vary the magnetic field of PQ2 from 0% to 100% of that of the regular operation. In the Y direction, the beam size gets larger as the PQ2 gets weaker since the PQ2 is the focusing magnet. On the other hand, in the X direction, the function has a minimum point. As a result, the precision of the measurement is better in the X direction case.

We estimate the amount of beam loss accompanied with this method. Fig.4.17 (a) shows the beam loss occurred between PQ2 and PC1. Fig.4.17 (b) shows the beam loss occurred elsewhere of the preparation section. With the magnetic field of PQ2 smaller than 0.2T/m, a part of the beam core is lost before the monitor, and the correct beam size cannot not be measured. We have to calculate the emittance using the magnetic field larger than 0.2T/m. If we should avoid the radiation in the downstream of the preparation section, we need to measure the emittance with the magnetic field of PQ2 larger than 0.8T/m. We calculate the emittance with the two conditions. The calculated emittance with the magnetic field of PQ2 larger than 0.2T/m is

$$\begin{aligned} \epsilon_x &= 6\pi \pm 0.42\pi \\ \epsilon_y &= 6\pi \pm 4.0\pi, \end{aligned}$$

and that with the magnetic field of PQ2 larger than 0.8T/m is

$$\begin{aligned} \epsilon_x &= 6\pi \pm 29\pi \\ \epsilon_y &= 6\pi \pm 9.4\pi. \end{aligned}$$

Both cases cannot satisfy the 10% measurement presicion requirement. The latter case gives very large error.

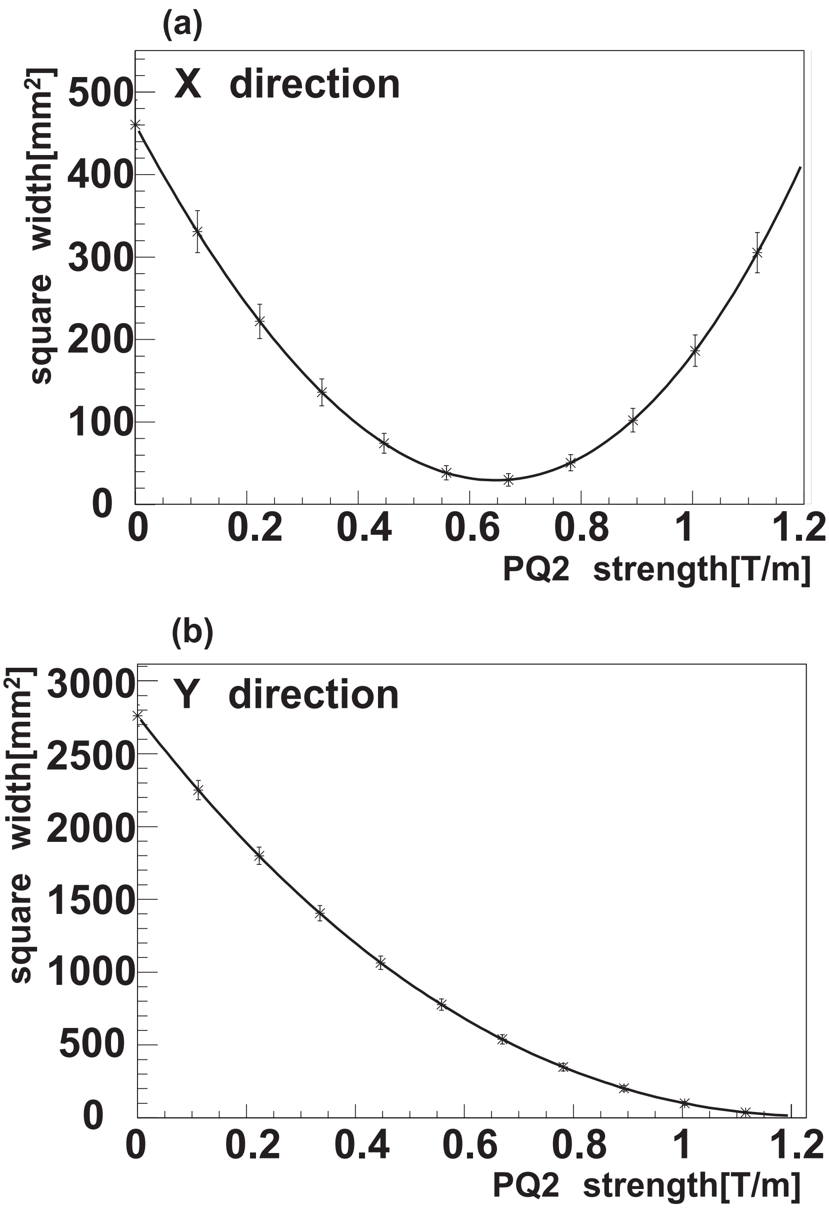

Figure 4.16: Beam sizes in front of PC1 corresponding to the various magnetic field of PQ2 in (a) X direction and (b) Y direction. The horizontal axis is the magnetic field gradient and the vertical one is the squared beam size.

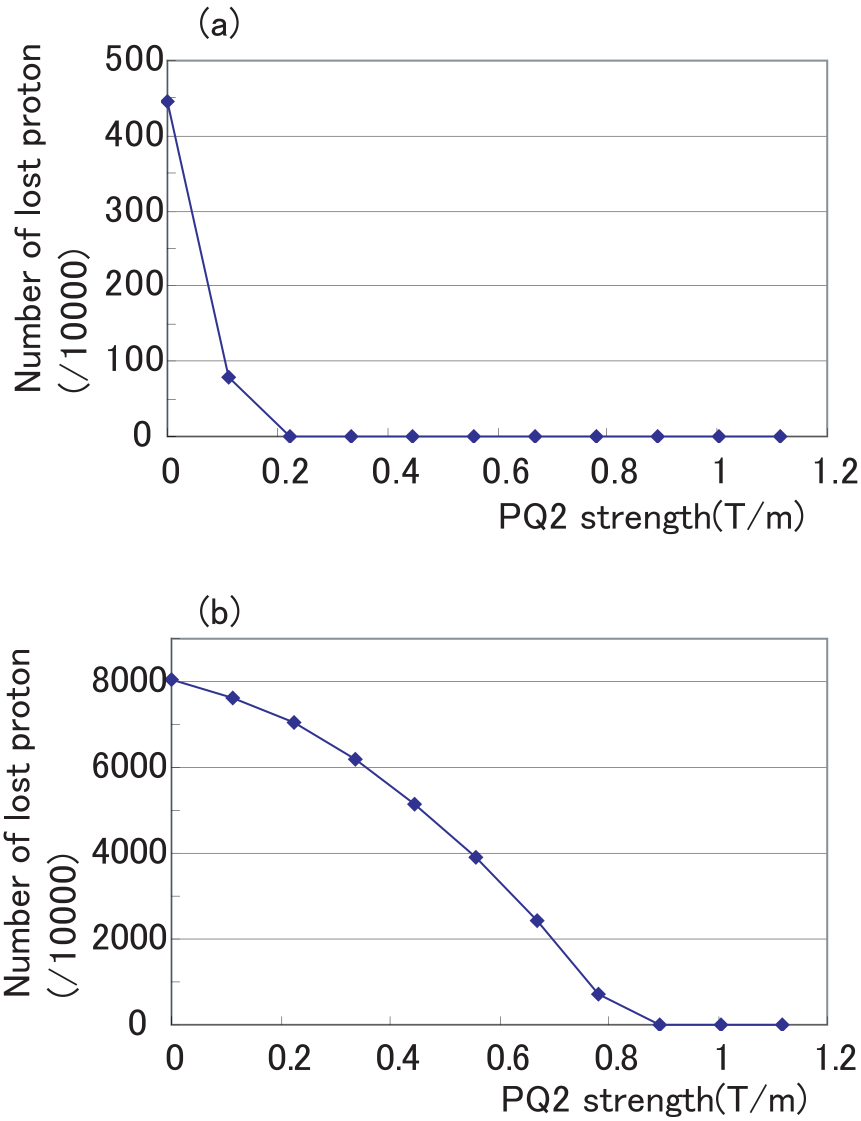

Figure 4.17: Number of the lost of protons per 10000 (a) before PC1, and (b) in the whole preparation section.

Method 3

Method 3 uses all monitors in the preparation section assuming the transfer matrix of the components. There is no hard beam loss, though we have to take account of the errors of quadrupole magnets.

We define $\alpha_0, \beta_0, \gamma_0$ as the twiss parameters at the extraction point, and the beam parameters at each monitor is expressed as

$$\begin{pmatrix} \epsilon\beta_i & -\epsilon\alpha_i \\ -\epsilon\alpha_i & \epsilon\gamma_i \end{pmatrix} = M_i \begin{pmatrix} \epsilon\beta_0 & -\epsilon\alpha_0 \\ -\epsilon\alpha_0 & \epsilon\gamma_0 \end{pmatrix} M_i^T \tag{4.3}$$

where $\epsilon\beta_i$ is the squared beam size at the ith monitor and M_i is the transfer matrix from the extraction point to the ith monitor.

Using the beam size data of nine monitors in the preparation section, we calculate the emittance by a least square method. We obtain

$$\begin{aligned} \epsilon_x &= 6\pi \pm 0.46\pi \\ \epsilon_y &= 6\pi \pm 0.56\pi. \end{aligned}$$

Here we obtain the good precision of less than 10% in both X and Y directions. In this calculation, we do not include the error of quadrupole magnets. Assuming the accuracy of the absolute quadrupole magnetic field as 0.1%, the error for the emittance is 0.04π for X, and 0.01π for Y. The dominant error source is from the resolution of beam monitors.

The effect of energy dispersion

In the X direction, the energy dispersion should be considered since it increase the beam size. (See Appendix B.) We compare the beam size evolution between the cases with the dispersion and without the dispersion as shown in Fig.4.18. The energy dispersion is 0.3% as shown in Table4.1. There is little difference, which is at most 0.2mm. The profile monitor, which has 0.7mm resolution, cannot recognize this difference.

We calculate the emittance with the dispersion using the Method 3, and obtain

$$\epsilon_x = 6.12\pi \pm 0.46\pi.$$

The difference from the real emittance is about 2%. The difference is considered as the error of the emittance measurement.

Short summary of the emittance measurement

Comparing these three methods, Method 3 is the only method that satisfy the 10% measurement precision requirement. We then choose the Method 3 to measure the emittance. The error of the measurement is estimated as follows,

$$\begin{aligned} \epsilon_x &= 6\pi \pm 0.46\pi \pm 0.04\pi \pm 0.12\pi \\ \epsilon_y &= 6\pi \pm 0.56\pi \pm 0.01\pi, \end{aligned}$$

where the first, second and third errors come from the resolution of monitor, the error of quadrupole magnets, and the effect of the energy dispersion, respectively. The following studies are carried out with the Method 3.

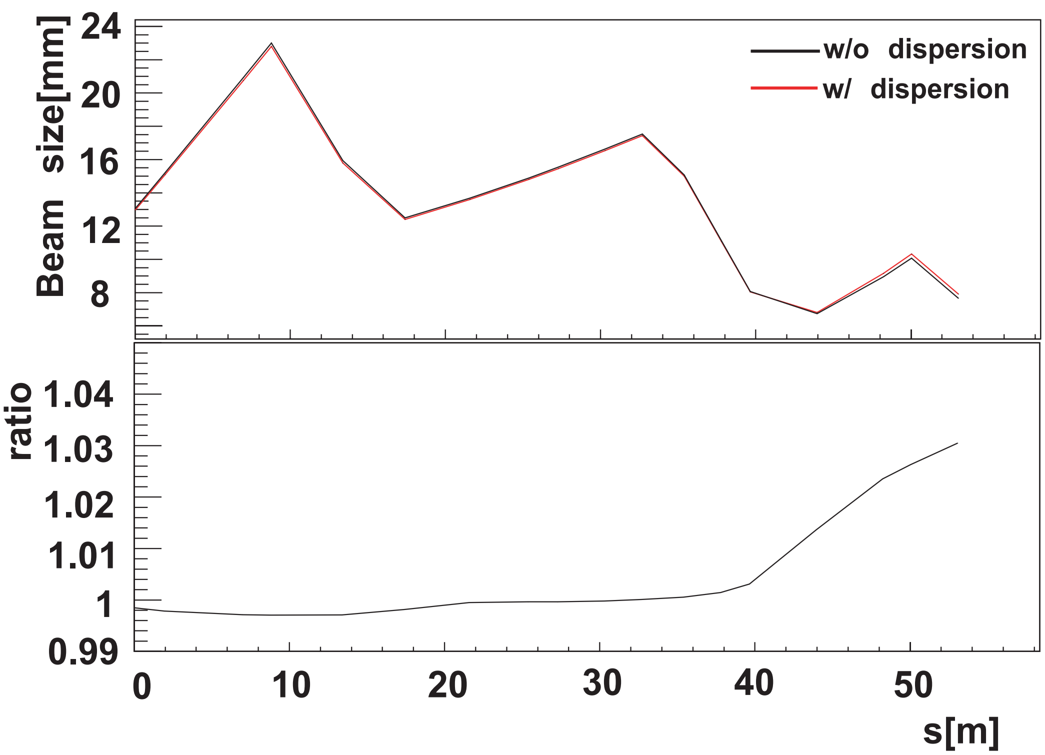

Figure 4.18: The upper figure is the evolution of the beam size along the preparation section. The red and black lines correspond to the beam sizes with the energy dispersion and without the energy dispersion, respectively. The lower figure is the ratio of the beam size with the dispersion to that without the dispersion.

4.6 Estimation of the Beam Size at the Target

A beam monitor cannot be installed just before the target since there is no free space around the target. We have to estimate the beam size at the target using the most downstream monitors, FM4 and FM5. The measured emittance is used for the estimation of the beam size at the target. The lower limit of the beam size to protect the target is 93% of the normal size [11]. We estimate the accuracy of the estimation of the beam size.

The following is the procedure to estimate the beam size at the target:

1. The emittance is measured at the preparation section,
2. The twiss parameters at the final two monitors are calculated using the measured beam sizes and emittance, and
3. The beam size is obtained by calculating the β function at the target.

In this section, we estimate the effect of the error of the emittance and the resolution of the final two monitors, respectively.

The effect of the error of the emittance measurement

The ideal beam size in the X direction at the final two monitors are 13.78mm and 13.34mm and the beam size at the target is 13.21mm for the 6π[mm$\cdot$ mrad] emittance beam. Fig.4.19 shows the error of the estimated beam size at the target in case that the emittance is wrongly measured. The beam size is correctly measured even if we take a wrong emittance. Since the measured value is the beam size ($\sqrt{\epsilon\beta}$), the β function is also wrongly calculated to cancel the error of the measured emittance.

The effect of the resolution of the profile monitor

The estimated accuracy of the beam size at the target is dominated not by the emittance measurement but by the resolution of the beam monitor. We define the accuracy of the beam size estimation as the maximum deviation of the beam width from the design optics when the beam width at the final two monitors deviates within the resolution of the beam monitors. With the current configuration of the beamline geometry, the accuracy of the beam size estimation at the target is 14%, which do not satisfy the requirement of less than 7%. The accuracy is improved if we put the final monitor close to the target. Fig.4.20 shows the accuracy of the beam size estimation as a function of the distance from the final monitor to the target. From this result, the distance from the monitor to the target must be less than 1.2m to satisfy the 7% accuracy.

4.7 Summary

In the J-PARC neutrino beamline, we should control the proton beam precisely to protect the components of the beamline and the target. To check the tuning scheme, we carry out the beamline simulations based on GEANT4.

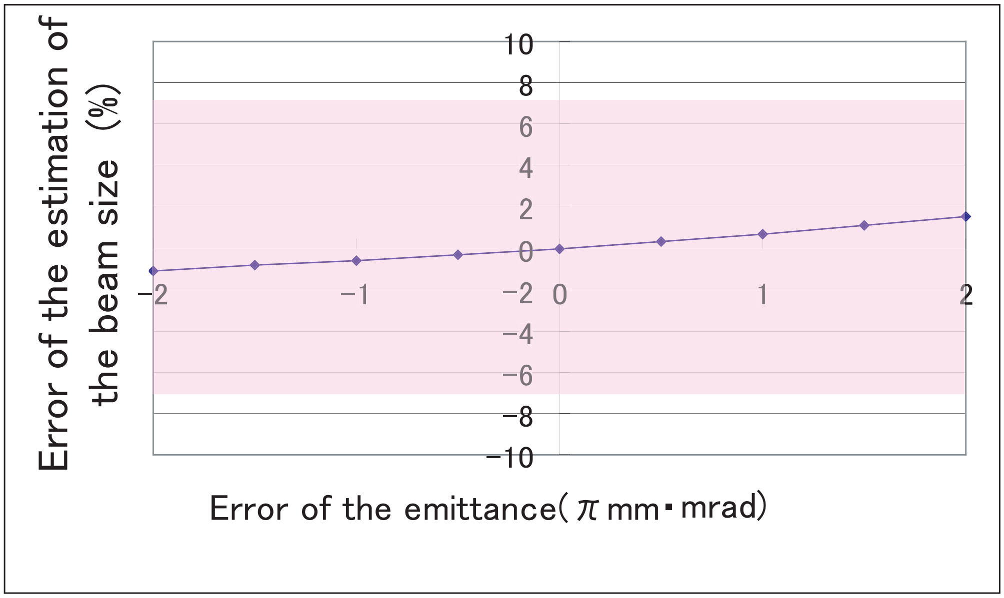

Figure 4.19: Relation between the error of the emittance measurement and the error of the estimated beam size at the target. The pink area is the requirement of the error of the estimated beam size.

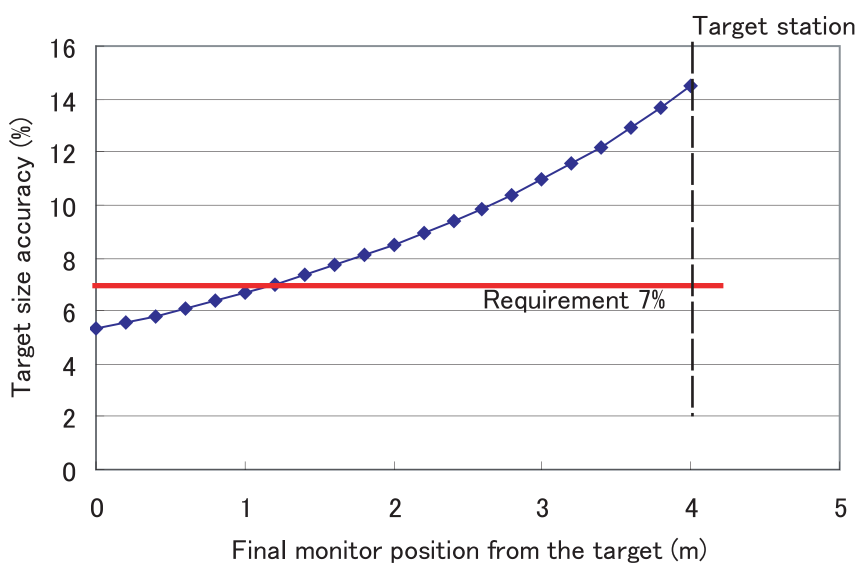

Figure 4.20: The relation between the position of the final profile monitor to the target and the accuracy of the beam size estimation.

First, we check the validity of the positions and the number of beam monitors and steering magnets which are used to tune the beam center position correctly. The resolution of the beam center position measurement is assumed to be 0.5mm. In the preparation section, we find additional two monitors should be installed before the PD1 and PV2 magnet. At the exit of the preparation section, the tuning accuracy is about 0.5mm in the X direction and 1.0mm in the Y direction. In the final focusing section, another vertical steering magnet should be installed. At the target, the tuning accuracy is about 0.8mm in the X direction and 2.8mm in the Y direction. The accuracy in the Y direction does not satisfy the requirement of 1mm. The poor accuracy in the Y direction is caused by the distance from the final beam monitor to the target. To obtain the required accuracy, it is required to put the monitor close to the target, and/or to improve the resolution of the beam monitor.

Second, we estimate the emittance measurement accuracy in the preparation section. Comparing three methods, we select the method to use all monitors in the preparation section. The emittance can be measured about 10% errors assuming the resolution of the profile measurement as 0.7mm.

The measured emittance is used for the estimation of the beam size at the target. We find the error of the emittance have little effect on the estimation. The resolution of the monitor is the dominant effect. With the current configuration, the accuracy of the beam size estimation is about 14%, though that the requirement is about 7%. It is required to set the monitor at less than 4m from the target.

Chapter 5

R&D of Residual Gas Beam Profile Monitor

To control the primary proton beam precisely, we install various beam monitors in the J-PARC neutrino beamline. Due to the very high intensity beam, the non-destructive beam monitors are desirable, since the destructive monitors will have short lifetime and make hard radiation loss. In addition, the monitors should cover the dynamic range of two orders of magnitude from $\sim 10^{12}$ppp (tuning or initial intensity) to $\sim 10^{14}$ ppp (full intensity).

The profile monitors are required to measure the beam profile with a resolution of less than 1mm. There are three candidates for the beam profile monitors: SSEM (Segmented Secondary Emission Monitor), Halo Monitor, and RGBPM (Residual Gas Beam Profile Monitor). SSEM is based on the phenomenon of secondary emission that occurs when the beam passes through the metal thin strip. Halo Monitor is based on the same principle of SSEM but measures only the beam halo, not the beam core. RGBPM utilizes the ionization of residual gas. Basically, SSEM is the first candidate to be installed and used along the whole beamline. However, SSEM cannot be used under the full intensity operation mode because of the large thermal stress on it. SSEM is, therefore, used under the low intensity mode and removed under the full intensity mode. On the other hand, we must measure the beam profile continuously in front of the target even in the full intensity operation mode to assure the beam size is not too small during the experiment. RGBPM is an alternative beam profile monitor for the constant use in the final focusing section. We have developed RGBPM as a candidate of this profile monitor.

In this chapter, we describe the R&D of RGBPM.

5.1 Principle of RGBPM

RGBPMs have been used as proton beam profile monitors at some proton accelerator facilities: the KEK-PS [12], RHIC [13], Fermilab [14], and so on. Fig.5.1 schematically shows the principle of RGBPM. Proton beams which pass through a beam duct ionize the residual gas. They produce pairs of positive ions and electrons. High voltage is applied between electrodes inside the vacuum chamber to make a uniform electric field. Along the electric field, the charged particles accelerate toward the upper electrode. By changing the polarity of the collecting high voltage, we can select electrons or positive ions as the collected particles. The collected charged particles are detected, multiplied, and converted to electric signals using the multi-anode MCP (Micro Channel Plate) [15, 16]. The amplitude of the output signals from each anode is proportional to the intensity of the incident proton beam at that point.

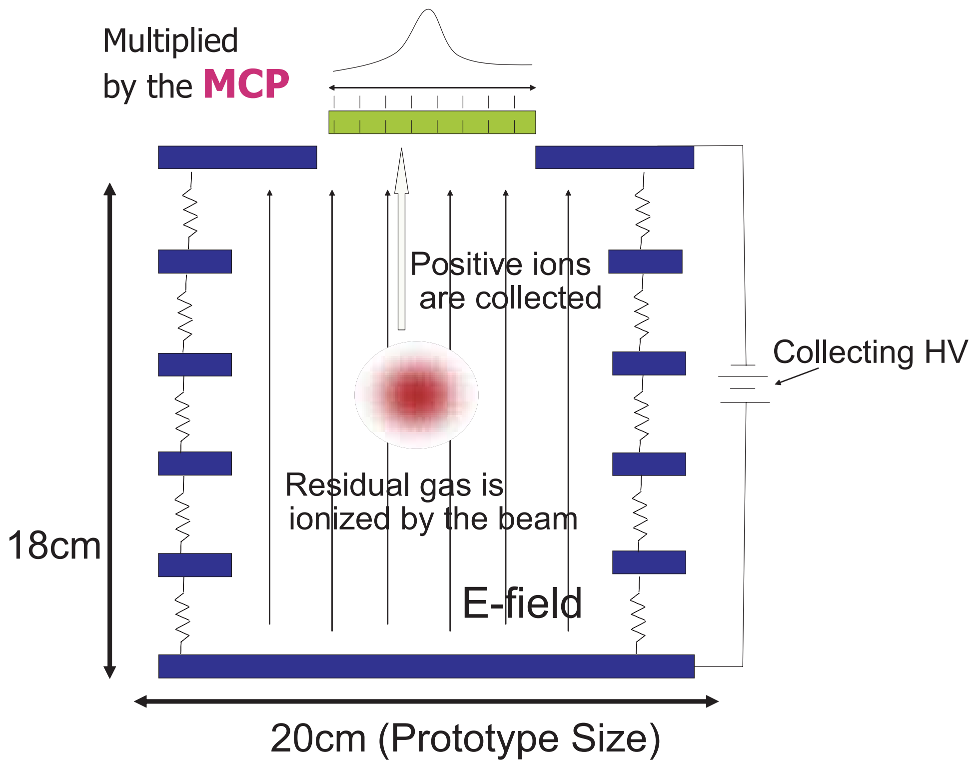

Figure 5.1: Schematic view of Residual Gas Beam Profile Monitor

The Micro Channel Plate (MCP)

An MCP is an array of fine lead glass pipes. Each pipe is called *a channel*. The inside wall of the pipe has resistant material which emits secondary electrons and make multiplication.

A high voltage ($\sim kV$) is applied between the MCP input surface and the output surface. Fig.5.2 shows how to multiply electrons from an incident particle:

1. An incident particle hits the entrance of MCP channel;
2. Secondary electrons are emitted;
3. The secondary electrons are accelerated by the electric field in the MCP;
4. The electrons hit the MCP wall and make another secondary electrons; and
5. Continue this process and the flow of amplified electrons are read out from the anodes.

The MCP is sensitive to electrons, ions, photons and so on. The typical gain is around 10^4. The gain increases up to 10^6 by combining two MCPs and up to more than 10^7 by combining three MCPs.

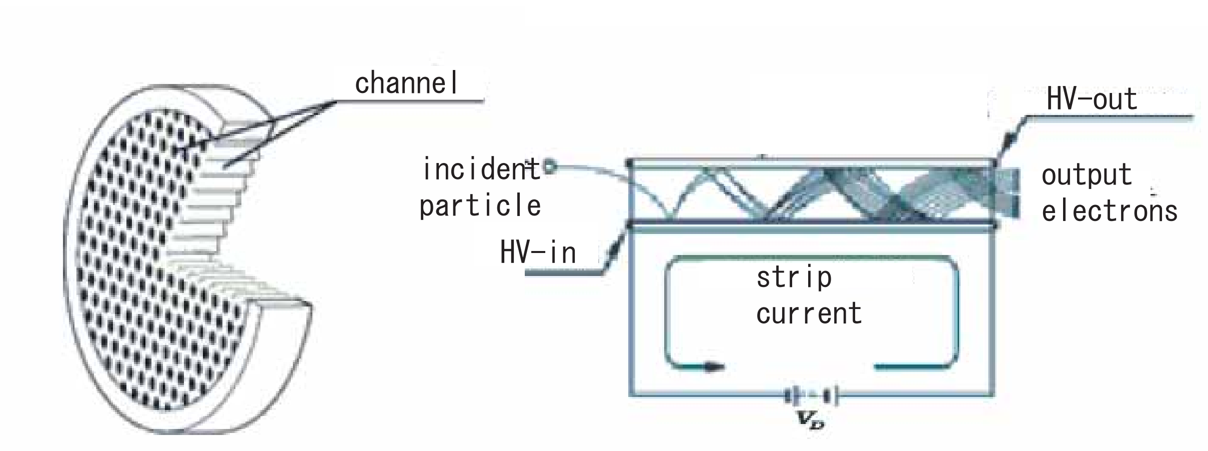

Figure 5.2: Multiplication scheme of the incident particle in a MCP channel

There are several devices to read out charged particles, such as a multi-anode EMT (Electron Multiplier Tube), segmented electrodes, and so on. Among them, we employ a MCP as a readout device for the following four reasons. First, since the neutrino beamline is under the high vacuum environment of 10^{-7} [torr] and the number of produced ion and electron pairs is limited, the gain of about 10^6 is required. Second, since the range of the beam intensity varies by two orders of magnitude, we need a device with a large dynamic range. We control the gain by changing the high voltage applied to the MCP. Third, a fine segmentation of anodes makes it possible to measure beam profiles. Fourth, MCP produces excellent results in the KEK-PS and so on.

5.2 RGBPM for J-PARC neutrino beamline

In the J-PARC neutrino beamline, the requirements for the beam profile monitors are as follows:

- The beam loss should be as small as possible;
- The position and profile resolution should be less than 1mm at the final focusing section; and
- The dynamic range should be covered from 10^{12} ppp to 10^{14} ppp.

The first criterion is satisfied since the RGBPM is non-destructive. The second requirement is satisfied by the anode segmentation with 2.5mm width (81mm per 32 anodes), which is much smaller than the beam size. The third is fulfilled by the high gain and large dynamic range of the MCP. There is another issue that the magnetic field is necessary to collect charged particles since the beam induced electric field is strong in the J-PARC neutrino beamline.

In this section, we discuss these requirements in detail.

The estimation of the amount of the signal

The amount of the signal per pulse is estimated from the degree of vacuum, the kinds of residual gas, the size of MCP, the gain of MCP, and so on. Assuming the parameters in Table.5.1, we estimate the size of the signal in the J-PARC neutrino beamline,

beam intensity	3.3×10^{14} ppp
vacuum in beam ducts	10^{-7}[Torr]
kind of residual gas	N_2
MCP gain	1×10^6

Table 5.1: Parameters assumed for the signal estimation.

We assume the energy loss of a proton in the N_2 gas to be 1.825[MeV/g/cm^2] and the density to be 1.25×10^{-3}[g/cm^3]. At first, the energy deposit of one proton in the gas is

$$\begin{aligned} dE &= 1.825[\mathrm{MeV/g/cm^2}] \cdot 3.1[\mathrm{cm}] \cdot 1.25 \times 10^{-3}[\mathrm{g/cm^3}] \cdot 1/760 \times 10^{-7}[\mathrm{Torr}] \\ &= 9.0 \times 10^7[\mathrm{eV/proton}]. \end{aligned}$$

Then since the ionization energy of nitrogen is about 35eV, the number of pairs of electrons and positive ions is

$$\begin{aligned} N_{pair} &= 9.0 \times 10^{-7}[\mathrm{eV/proton}]/35[\mathrm{eV/ion}] \cdot 3.3 \times 10^{14}[\mathrm{proton/pulse}] \\ &= 8.4 \times 10^7[\mathrm{ion/pulse}] \end{aligned}$$

By multiplying the gain of MCP, the estimated total signal is about

$$8.4 \times 10^7[\mathrm{ion/pulse}] \cdot 10^6 \cdot 1.6 \times 10^{-19} = 13[\mu\mathrm{C}]. \tag{5.1}$$

This value is large enough that the signal is read out successfully even if the beam intensity is two orders lower.

The electric field induced by the proton beam

In the J-PARC neutrino beamline, since the density of the fast extracted proton beam is very high, the electric field induced by the proton beam itself cannot be ignored compared with the collecting field. Here, we estimate the electric field of the proton beam.

The electric potential is expressed as follows,

$$V(x,y) = \frac{N}{\Delta t}\frac{e^2}{2\pi\epsilon_0 v_p}\int_{-\infty}^{\infty} dx' \int_{-\infty}^{\infty} dy' \rho(x',y') \log\{(x-x')^2 + (y-y')^2\}/2, \tag{5.2}$$

where N is the number of protons per bunch, Δt is the bunch width (time), v_p is the velocity of protons, ρ is the function of the proton beam density. We assume that the

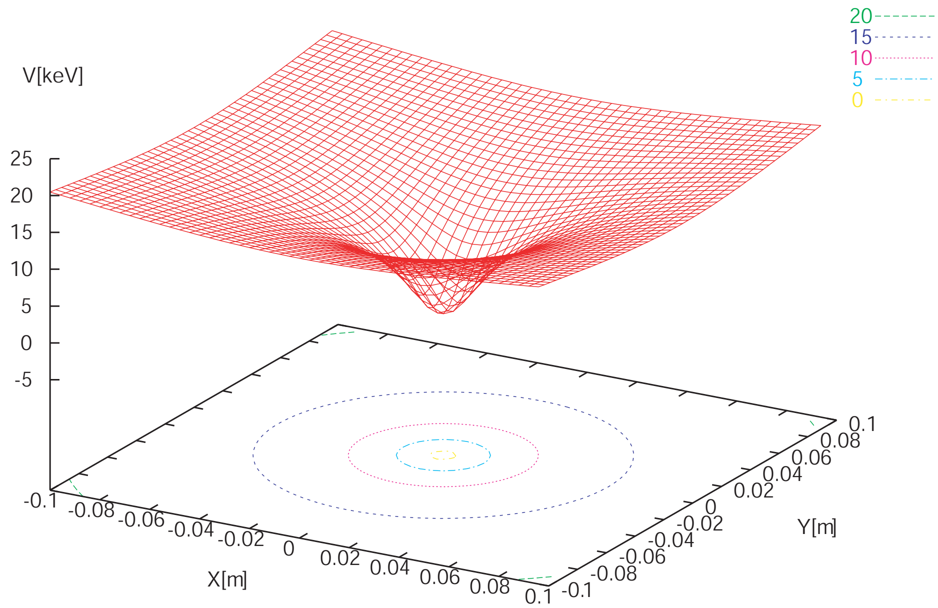

Figure 5.3: Calculated electrical potential of the J-PARC proton beam.

beam has a Gaussian distribution and its σ is 7mm for both vertical and horizontal directions. Fig.5.3 shows the calculated electric potential produced by the proton beam. The typical strength of the electric field is about 250kV/m around the beam. This value is very large and it is difficult to apply much higher voltage to our electrodes.

We perform a simulation of the motion of particles in the electric field made by the proton beam and by collecting electrodes. In the simulation, we put a uniform electric field and the proton beam induced field. An ion (H_2O^+) or an electron produced at (7mm, 7mm) moves in these electric fields during the bunch width ($\sim$50ns).

Fig.5.4 (a) shows the tracking result for an electron. Due to the beam induced electric potential which gives kinetic energy, the electron moves around the beam as shown in the Fig.5.4 (a), and already has no information about its produced position. To suppress the horizontal movement of the electron, we also apply a magnetic field that is parallel to the collecting electric field. As shown in Fig.5.5, charged particles coil along the line of the magnetic force with the larmor radius. Fig.5.4 (b)-(d) show the tracking results for an electron with various strength of a magnetic field. With strong magnetic field, the horizontal movement of the electron is restricted. After the beam passes through, the electron is collected by the collecting electric field. About 0.05T is necessary to keep the horizontal position of the electron within one anode of MCP.

We also simulate the motion of a positive ion as shown in Fig.5.6. The length of the track is small because of its heavy mass. Without the magnetic field, however, the positive ion is scattered about 2.5mm in horizontal. The ion will move more until it reach MCP since the horizontal velocity is large. Even applying a magnetic field of 0.1T, the horizontal movement is not suppressed since a massive particle has a large larmor radius. To obtain the 1mm larmor radius, we must apply about 5T or more magnetic field if we collect the positive ions to measure the beam profile in J-PARC.

This simulation indicates it is difficult to use the positive ion collection to measure

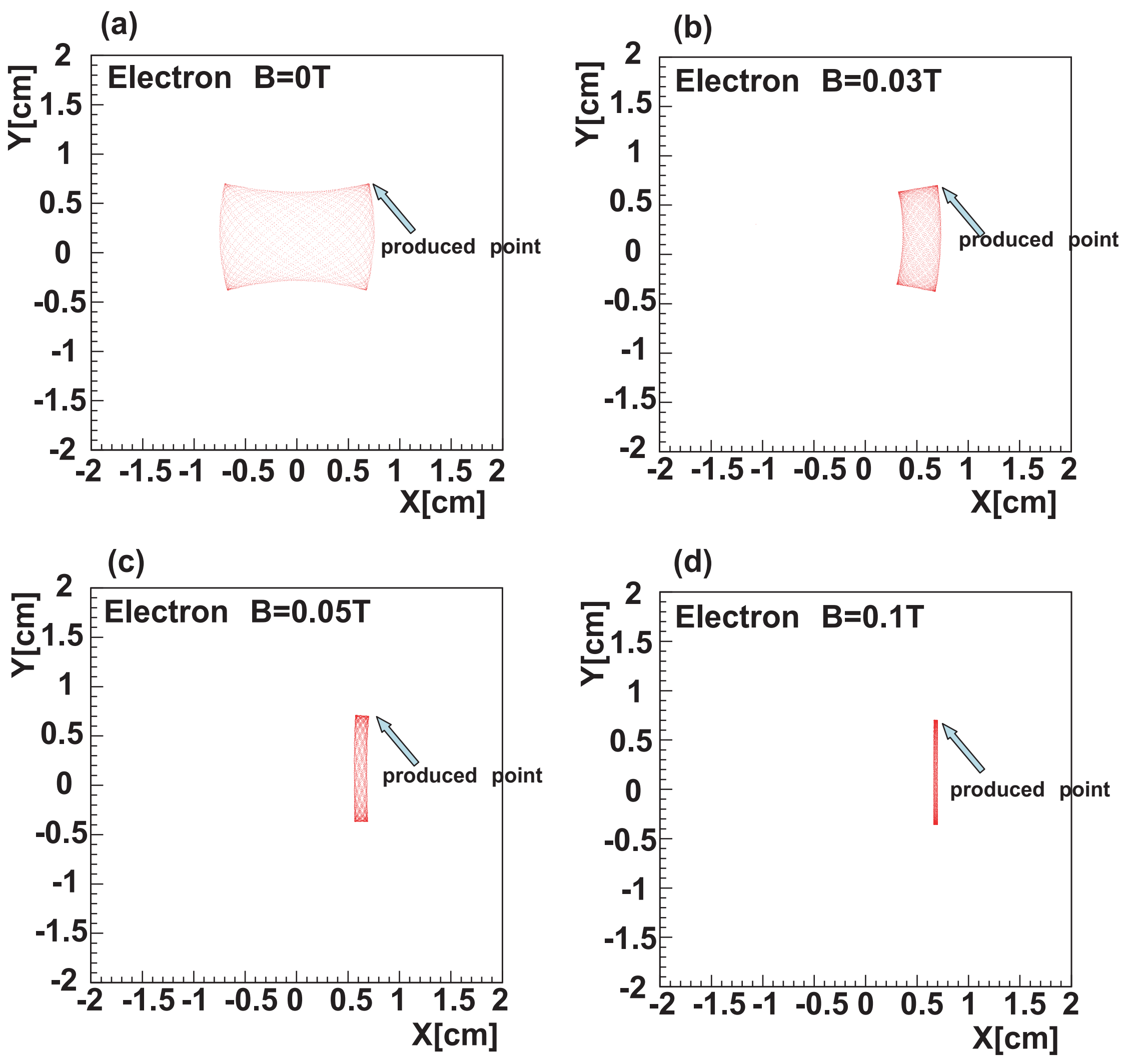

Figure 5.4: Tracks of an electron produced at (7mm, 7mm). We applied collecting electric field (100kV/m), beam-induced field and a external magnetic field. The applied magnetic field is (a) 0T, (b) 0.03T, (c) 0.05T, and (d) 0.1T.

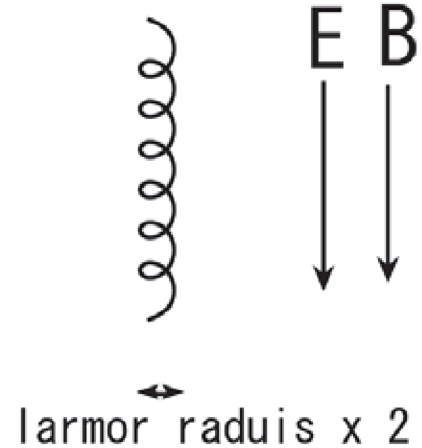

Figure 5.5: Schematic track of charged particle in parallel electric and magnetic field.

the beam profile, because it required the high magnetic field to keep the beam profile, and thus the electron collection with a sufficient magnetic field is necessary.

5.3 Beam test at K2K neutrino beamline

We carry out beam test at the K2K neutrino beamline. The aim of the beam test is to check the basic performance of RGBPM under the magnetic field. The proton beam is fast extracted from the KEK-PS to the K2K neutrino beamline keeping a multi-bunch structure. The parameters of the beam are similar as the J-PARC proton beam for T2K experiment except for the intensity and energy.

5.3.1 Setup

At first, we make a prototype of RGBPM for the beam test. As a readout device, F2813-22MX MCP made by Hamamatsu Photonics K.K. is chosen since this model has two stages of rectangular MCP and the gain is $10^6 \sim 10^7$. The sensitive area is 81mm $\times$ 31mm. The anode is segmented into 32 channels for the transverse direction of the beam and this segmentation enables us to measure the beam profile. Fig.5.7 shows a photograph of the MCP used for the present RGBPM.

We make a vacuum chamber for the MCP and the electrodes. The electrodes for the collecting electric field are made of aluminum and consist of five stages. The sizes of the electrodes are 16cm wide, 16cm height, and 10cm long, which are larger enough than the beam size. The vacuum chamber for the MCP and the electrodes has been made. The vacuum degree of the K2K beamline is about 10^{-2}[torr]. Since the MCP must be operated under the high vacuum environment which is less than 10^{-5}[torr], the beamline and our vacuum chamber are separated by 50μm thick foils made of SUS. Fig.5.8 is the picture of the MCP and the electrodes in the vacuum chamber.

Next, we install this prototype into the K2K beamline (Fig.5.9). To check the operation in a magnetic field, we replace an existing steering dipole magnet to the one which

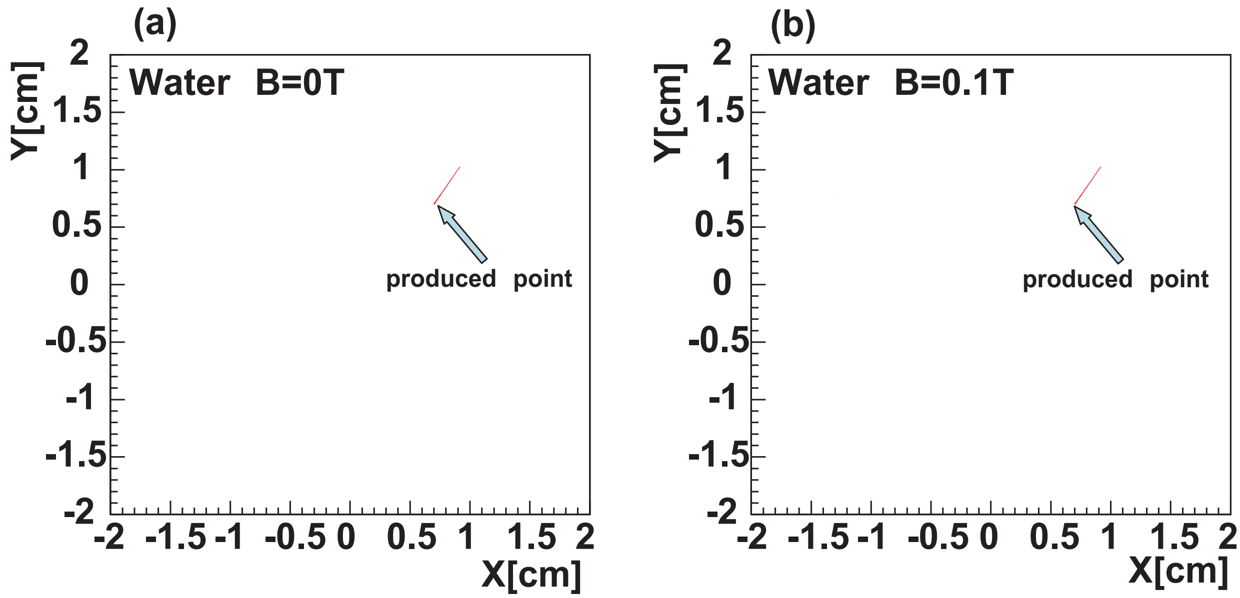

Figure 5.6: Tracks of an ion(H_2O^+) produced at (7mm, 7mm). We applied collecting electric field (100kV/m), beam-induced field and a external magnetic field. The applied magnetic field is (a) 0T and (b) 0.1T.

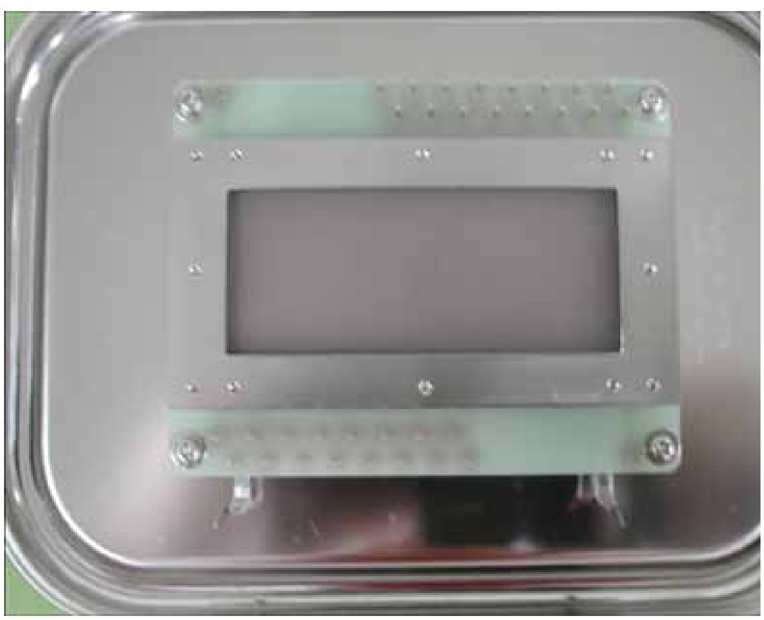

Figure 5.7: The multi-anode Micro Channel Plate

has a larger vertical gap of 30cm and put the monitor into the gap. The magnet generates a magnetic field with the range of the strength from -0.3T to 0.3T, which covers enough range for our test since the intensity of the beam is two orders lower than that of the J-PARC proton beam. The schematic view of the installation is shown in Fig.5.10. The high voltage coaxial cables for the MCP and the electrodes and the 32ch twisted cables for signals are installed and connect the control area which is located 40m from the monitor. The signal is read out and analyzed with an oscilloscope and FASTBUS ADC.

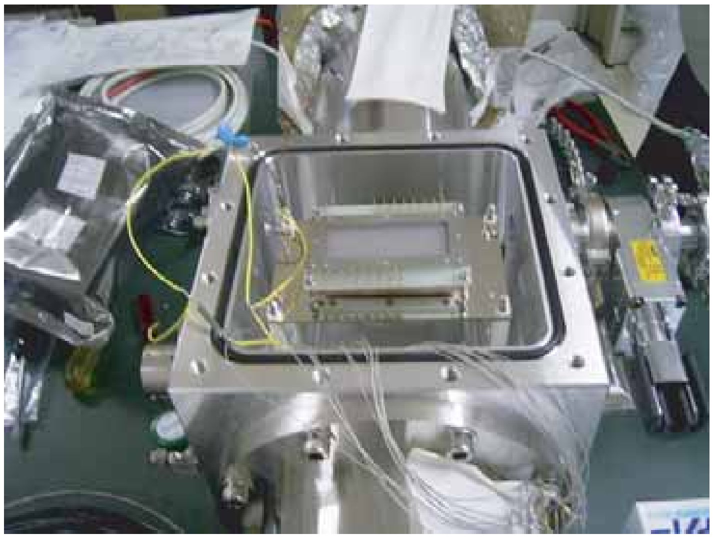

Figure 5.8: Vacuum chamber and detector.

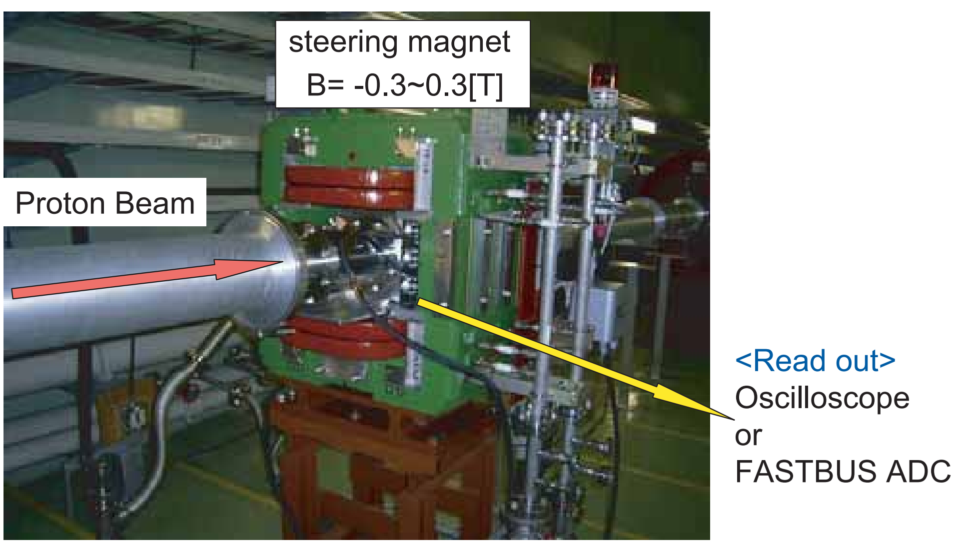

Figure 5.9: Monitor installation into the K2K beamline.

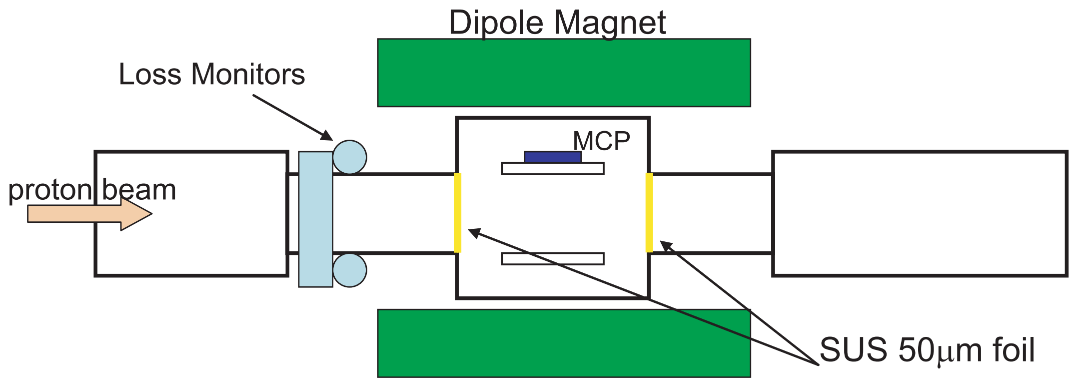

Figure 5.10: Schematic view of the installation of RGBPM

5.3.2 Results of the beam test

Performance of RGBPM

The results of the beam test are described below. Fig.5.11 shows the measured signal of RGBPM. The three lines correspond to the signals from different MCP channels. The applied electric field is 10kV/m and the applied magnetic field is 0.03T. These signals synchronize with the beam timing trigger and have nine peak structure. This corresponds to the K2K beam structure. The signals disappear by turning off the high voltage of MCP. We confirm that MCP amplifies the signal properly with the applied high voltage.

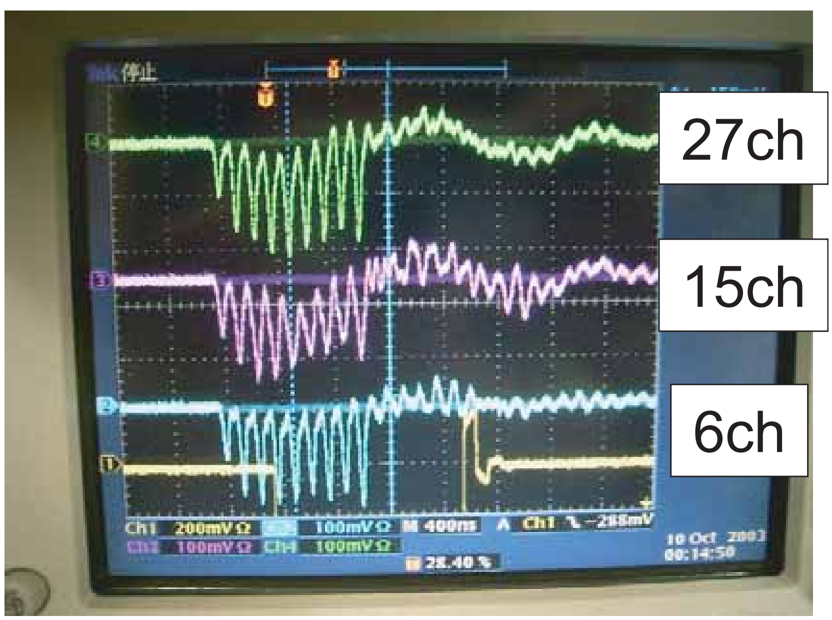

Figure 5.11: Signals of RGBPM at the K2K beam test.

Next we measure the beam profile using a 32ch charge sensitive ADC. We open the ADC gate to accept the nine peaks which correspond to fast electrons. Fig.5.12 shows the measured beam profiles. The red, green and blue lines correspond to the profiles with the electron collecting field, no electric field and electron rejection field, respectively. Each profile is normalized by the beam intensity measured by the nearby intensity monitor. There is some response to the change of collecting field. The amounts of the signals per channel are, however, more than 10 times larger than our estimation, which is less than 100 ADC count. We doubt a large background disturbs the measurement of the beam profiles. We cannot check the performance of RGBPM under the magnetic field due to the large background.

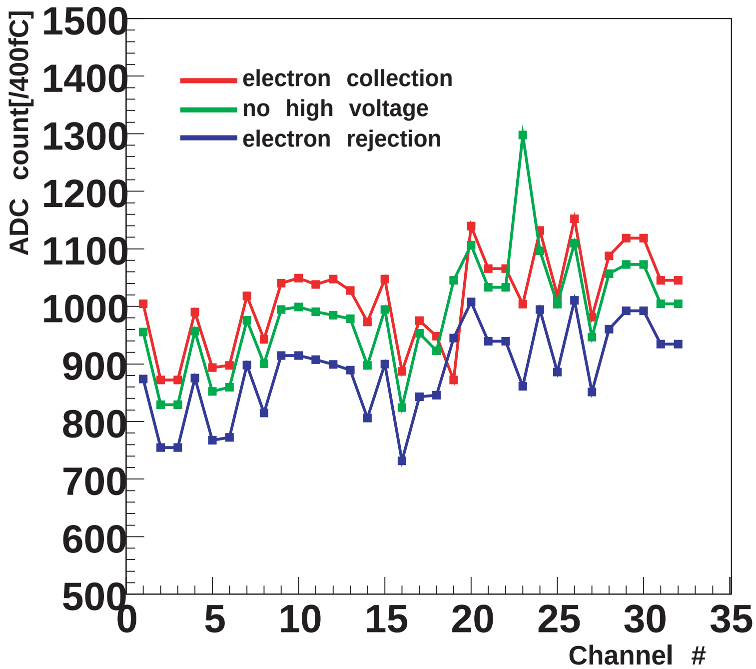

Figure 5.12: Measured beam profile at K2K beamline. The horizontal axis is the position and the vertical one is the ADC count. The red, green, and blue lines indicate the profiles with the electron collection field, without the collection field, and the electron rejection field.

Beam loss measurement

To make sure if the large background is caused by real particles or not, we measure the beam loss/shower around RGBPM. We install four beam loss monitors in front of RGBPM as shown in Fig.5.13. Fig.5.14 shows the signals of the beam loss monitors. The amount of the signals is typically 50nC per one monitor per pulse. The same beam loss monitors are also installed into another accelerator and beamline in the KEK-PS where the profile monitors using ionization of residual gas work well. The amounts of signal at these beamlines are typically several tens of pico coulomb. We find RGBPM works in the beamline which has little beam loss. This result strongly indicates that there is large background around our beamline caused by the beam loss and/or shower.

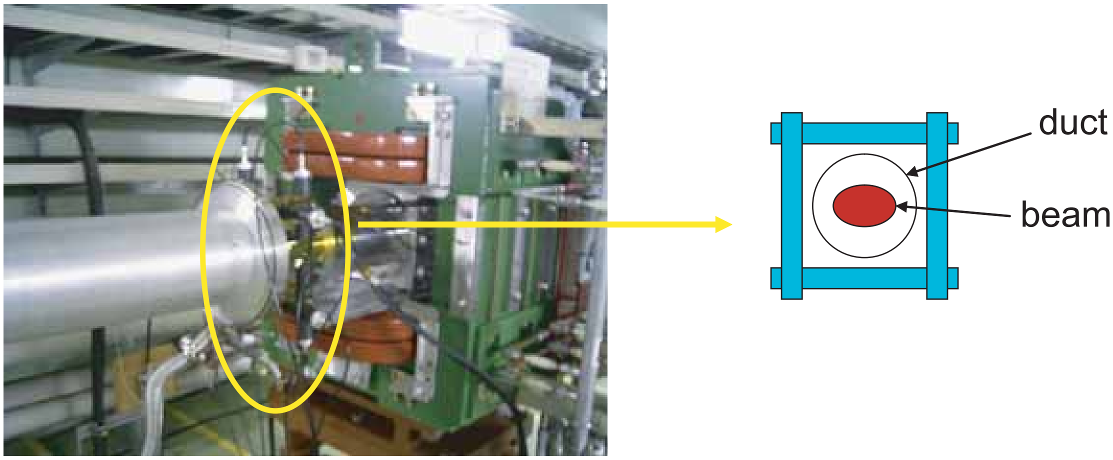

Figure 5.13: Installation of beam loss monitors around the beam duct.

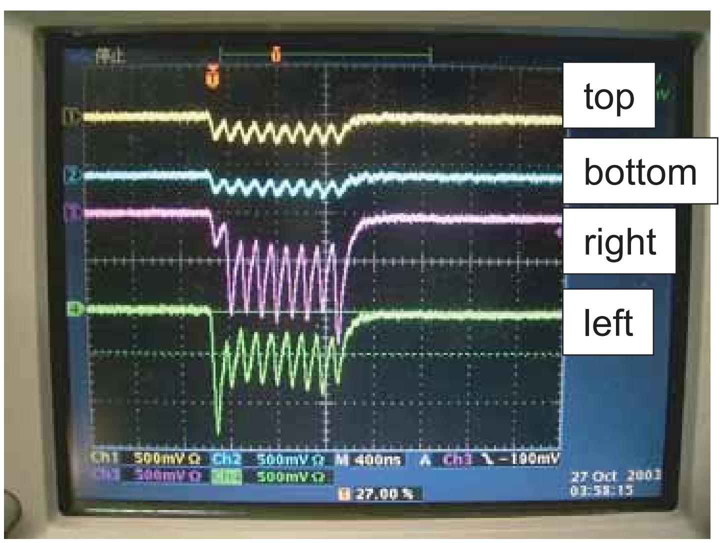

Figure 5.14: Signals of beam loss monitors. The four lines indicate the signals from the top, bottom, right and left beam loss monitors.

5.4 Beam test at NML Beamline

In the beam test at the K2K neutrino beamline, we cannot observe the proton beam profile because of the larger background than signal. We have made another prototype and carry out the beam test at the NML proton beamline. The tests have two purposes. First is to observe the clear beam profile and obtain the basic data under the normal RGBPM operation. Second is to make an artificial background and to examine the response of RGBPM under the large background environment. Considering these test results, we should determine if RGBPM is feasible for the J-PARC neutrino beamline.

The NML beamline is an extracted line from the Booster ring of KEK-PS. It supplies a proton beam for neutron and meson experiments. The comparison of the K2K neutrino beamline and the NML beamline is shown in the Table5.2.

	K2K neutrino beamline	NML beamline
Beam Energy [GeV]	12	0.5
Beam Intensity [ppp]	6.6×10^{12}	2.5×10^{12}
Repetition Rate [Hz]	0.46	20
Number of bunches	9	1
Vacuum rate[torr]	$\sim 10^{-2}$	$\sim 10^{-7}$
Beam loss[nC]	~ 50	~ 0.025
Beam size(mm)	40	15

Table 5.2: Comparison of the K2K neutrino beamline and the NML beamline

The NML beamline has several advantages:

- It has very small beam loss;
- Since the monitor is expected to work well in this line, we can observe the fundamental operations of the beam monitor except for the multi-bunch effect; and
- It is not needed to separate the vacuum because the beamline itself is under the high vacuum.

5.4.1 Setup

For the test, we make a new prototype detector. The basic design is the same as that of the previous beam test in the K2K beamline. To simplify the monitor configuration and to observe the effect of beam loss, we apply modifications to the new detector. The differences from the first beam test are:

- Magnetic field is removed;
- Electric field is stronger than previous (10kV/m $\rightarrow$ 50kV/m); and
- Set the aluminum cover around the MCP to protect from the beam loss.

Fig.5.15 and Fig.5.16 show the pictures of the installed RGBPM (in the vacuum chamber) and the inner electrodes of RGBPM, respectively.

In this test, various properties of RGBPM are studied: the relation between RGBPM and the beam induced background, and the collecting high voltage dependence of the measured beam profile width. To study the relation between signals from RGBPM and beam induced background, we install a beam loss monitor (shown in the Fig. 5.15) measuring the beam induced background around RGBPM. To study the beam background properties in detail, we put a 1mm-thick aluminum board across the beam to generate particle showers from the proton beam (Fig.5.17). The particle showers are detected by the beam loss monitor, to estimate the relation between RGBPM and beam loss.

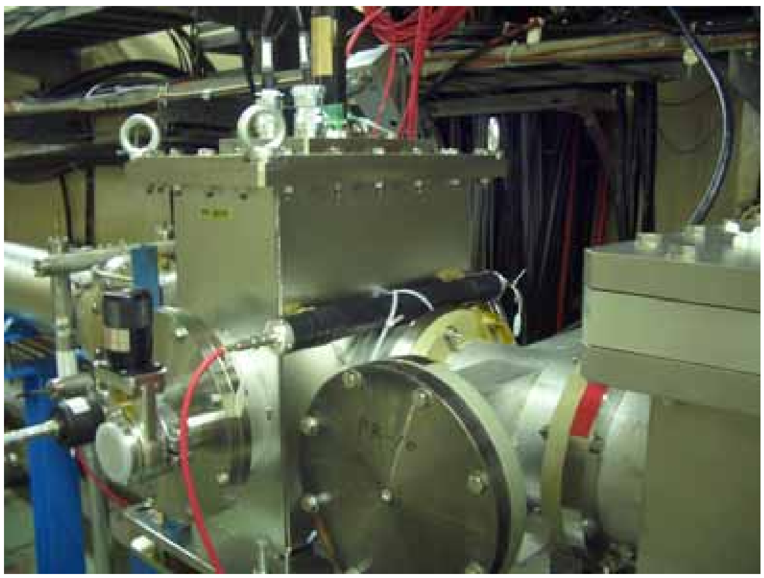

Figure 5.15: Installed RGBPM (in the vacuum chamber) and a Beam Loss Monitor (the black bar)

5.4.2 Results of the beam test

Signal of RGBPM

The typical signal of positive ions is measured as shown in Fig.5.18. The applied collecting high voltage is 10kV/180mm. There are clear three peaks originated from three kinds of positive ions. Since these ions have different mass numbers, the drift time, which is the time between the beam timing and the peak, differs among ion species. Fig.5.19 shows the relation between the collecting high voltage and the drift time of ion. The three lines correspond to the three peaks in Fig.5.18. The lines show that the drift times get smaller as the high voltage gets higher. By fitting the data points of the drift time, we calculate the mass number for each ion and identify its species.

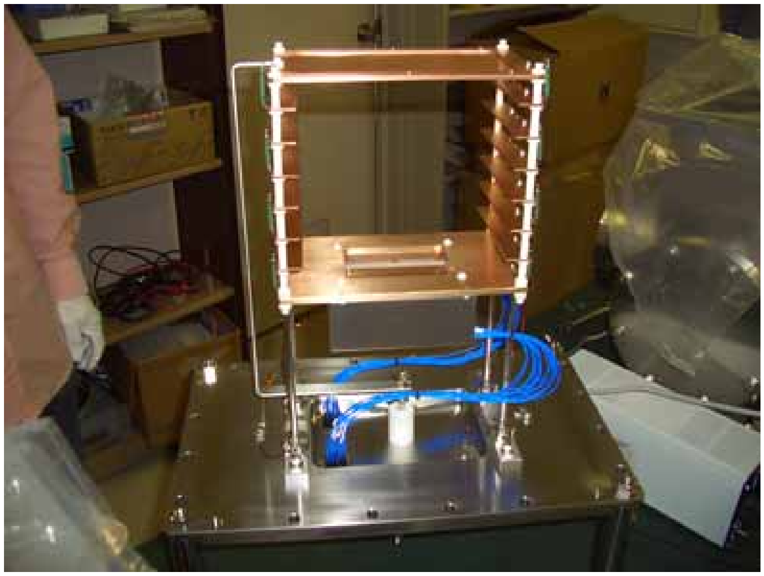

Figure 5.16: Inner electrodes of RGBPM and MCP (in the Al shield)

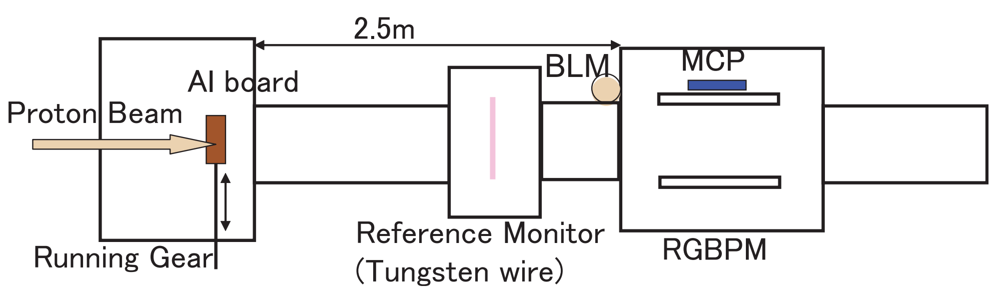

Figure 5.17: Schematic view of the interrupting Al board and the running gear.

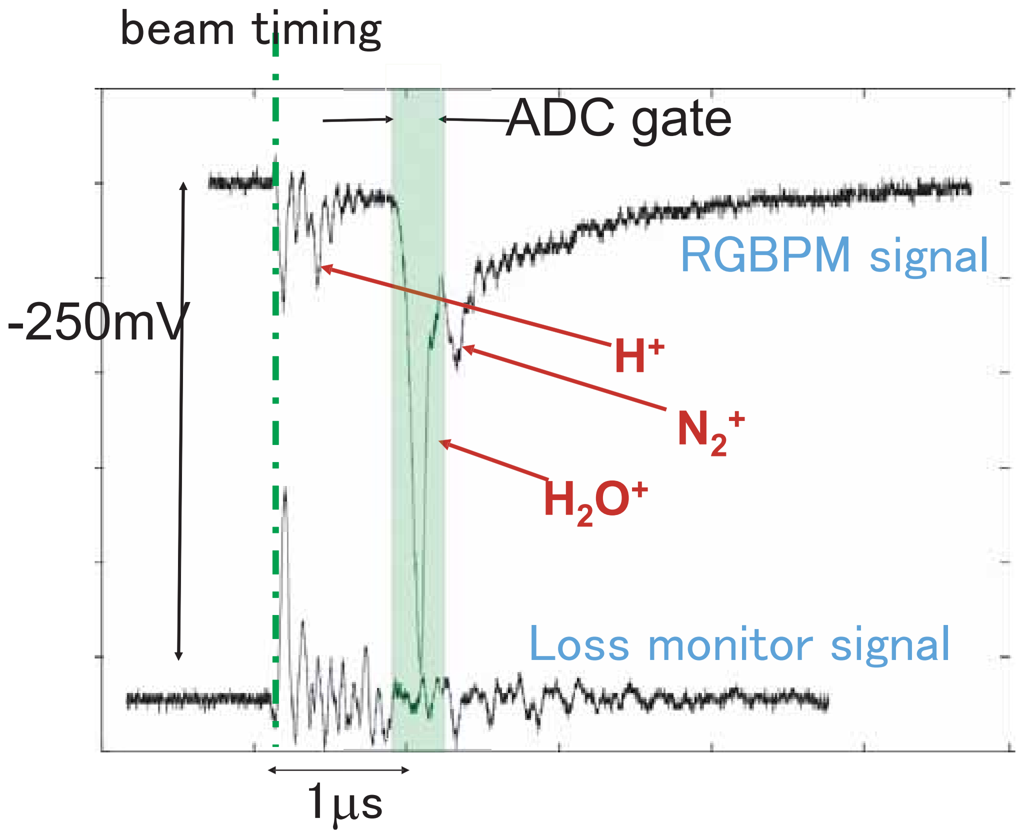

Figure 5.18: (Upper) Typical signal of RGBPM applied 10kV collecting high voltage. (Lower) Signal of the beam loss monitor with artificial beam loss.

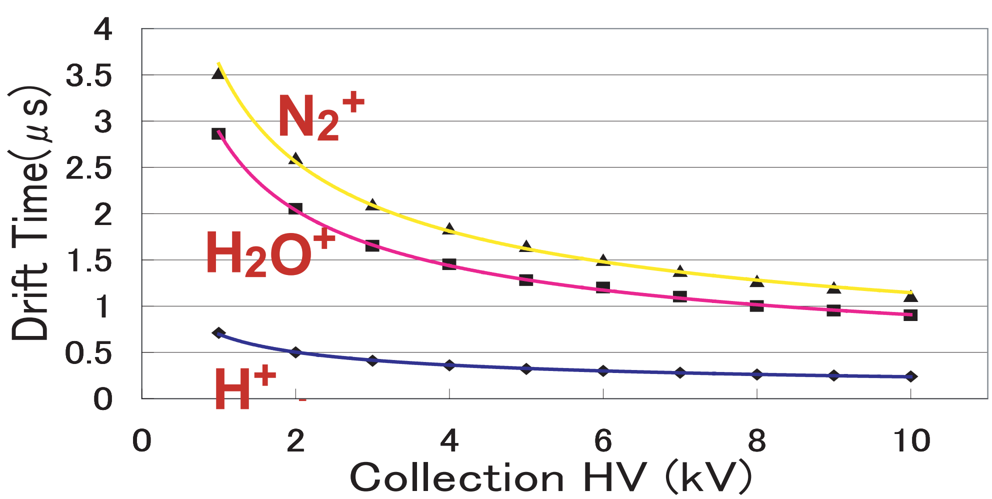

Figure 5.19: Collecting high voltage dependence of drift time of ions. Each of three lines indicates H^+, H_2O^+ and N_2^+ from bottom to top.

Profile measurement

For the data taking, we use a 32ch charge sensitive ADC and open the gate around the largest peak (H_2O^+ peak), which corresponds to the green hatched area in Fig.5.18. Fig.5.20 shows the measured beam profiles. The blue and red lines show the profiles measured by our RGBPM and a wire profile monitor (reference monitor) respectively. Each monitor has 2.5mm width per channel. By fitting these distributions with a Gaussian function, we calculate the center and width. Obtained widths are consistent within a precision of 20 % (Table 5.3).

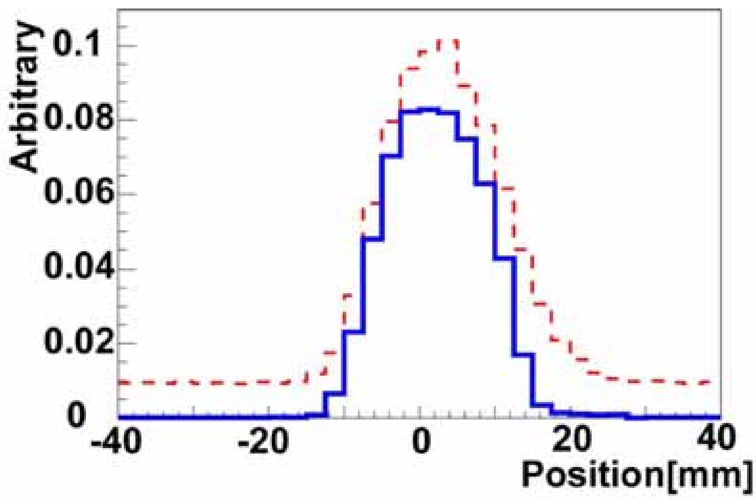

Figure 5.20: The measured beam profile with ion collecting mode (blue) and the reference profile measured by the wire monitor (red).

Table 5.3: Measured beam parameters by RGBPM and reference monitor

	RGBPM	Reference(wire monitor)
Beam Center	+2.9mm	+3.3mm
Beam Width	5.9mm	7.1mm

To verify the profile measurements, we vary the beam center and width, and measure the profiles. Fig.5.21 shows the comparison between the normal beam profiles and the varied beam profiles. The blue and purple lines indicate the profiles of the normal beam and the varied beam, respectively. The upper figure corresponds to the change of beam center, while the lower figure corresponds to the change of beam width. The changed beam profiles are checked by the other monitor for the beam center, and by optics calculation for the beam width. We find RGBPM shows the proper response as a profile monitor.

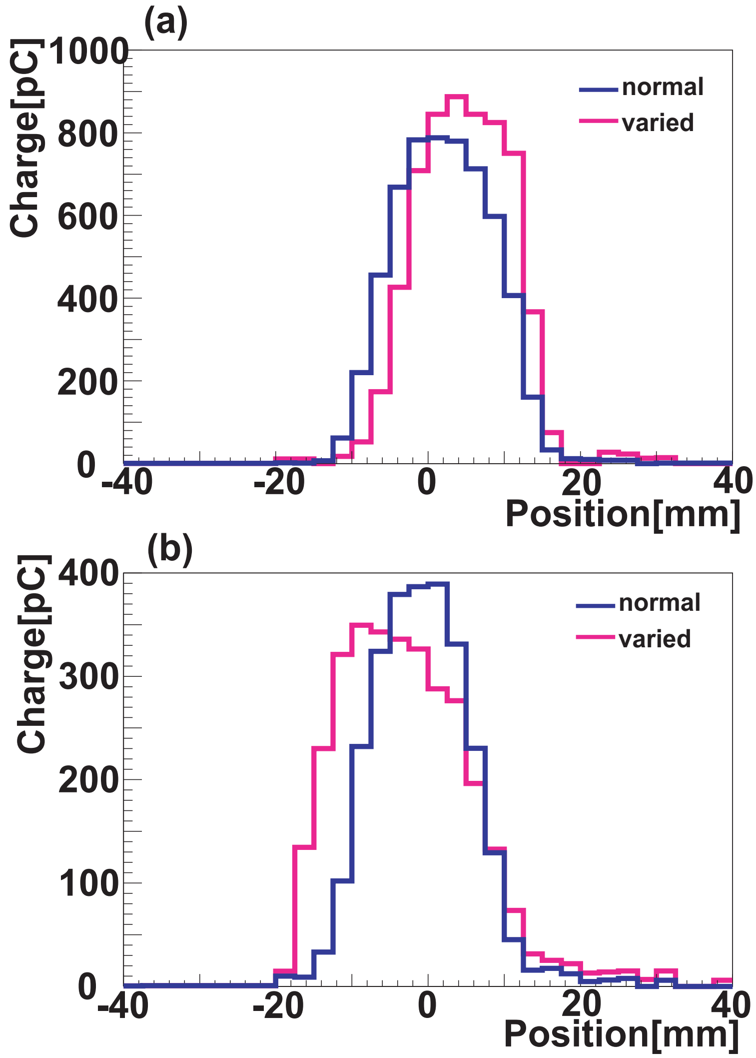

Figure 5.21: Comparisons of the normal beam profile and the varied beam profile. We change (a) the center with the dipole magnet and (b) the width with the quadrupole magnet.

Timing of signal and background

Changing the polarity of the collecting high voltage, we also measure the beam profile by the electron collection. The ADC gate is opened at the beam timing because the signal from electrons is coincident with the beam timing within a few nanoseconds. Fig.5.22 shows the measured beam profiles for the electron collection. The green and purple lines indicate the profiles with a -6kV collection high voltage and without the collection high voltage, respectively. We consider the profile without the collection high voltage represents the profile of the beam induced background. The result indicates that the measured profile consists with the profile of the beam signal and that of the beam induced background.

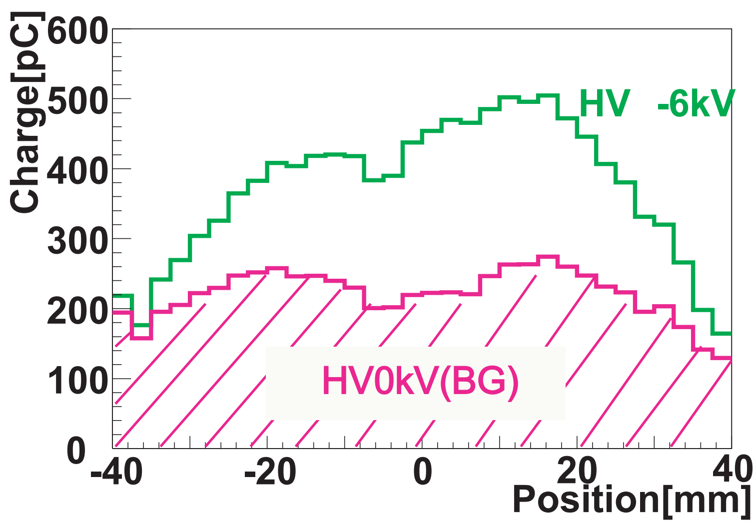

Figure 5.22: Measured profile with electron collection mode (green) and without the collecting high voltage (violet).

For the further study of the effect of the beam induced background, we artificially increase the beam loss and measure it with the beam loss monitor. The lower line in Fig.5.18 shows the signal from the beam loss monitor. We find that the beam induced background signal comes at the same timing with the beam, and that the profile with the electron collection is influenced by the beam induced background. To the contrary, the ion signals have delay from the beam timing, because of its heavier mass. Thus, the profile measurement with the positive ion collection can avoid the beam induced background. Under the high beam induced background environments, such as the J-PARC neutrino beamline, it is necessary to collect the positive ions and avoid the beam induced background in the RGBPM operation.

Beam induced electric field

The final result is the effect of the beam induced electric field. We check the measured beam width variation by changing the collecting high voltage. Fig.5.23 shows the dependence of the width of the measured beam profile on the collecting high voltage. The width decreases as the high voltage increases up to 3kV. This beamline has 2.5×10^{12} ppp intensity, which typically produces about 10kV/m electric field. Since the electric field induced by the proton beam disturbs the collecting field and the ionized particles are scattered radially. The collecting field must be, therefore, large enough compared with the beam induced field. We estimate that RGBPM works under the beam induced electric field of less than about 20kV/m.

5.4.3 Discussion on the feasibility of RGBPM for the J-PARC neutrino beamline

From the results of the beam test at the NML beamline, we get basic information to discuss the RGBPM usage in the J-PARC neutrino beamline. We find that the electron collecting mode is difficult under the large beam-induced background environment since the background comes at the same timing with the signal of RGBPM. The positive ion collecting mode is, however, impossible since the ions are scattered by the strong beam-induced electric field without the incredibly large magnetic field parallel to the collecting field.

It is considered that the fast extracted beam in J-PARC have large beam-induced background and high beam-induced electric field due to the high intensity. We summarize that RGBPM is not suitable for the J-PARC neutrino beamline.

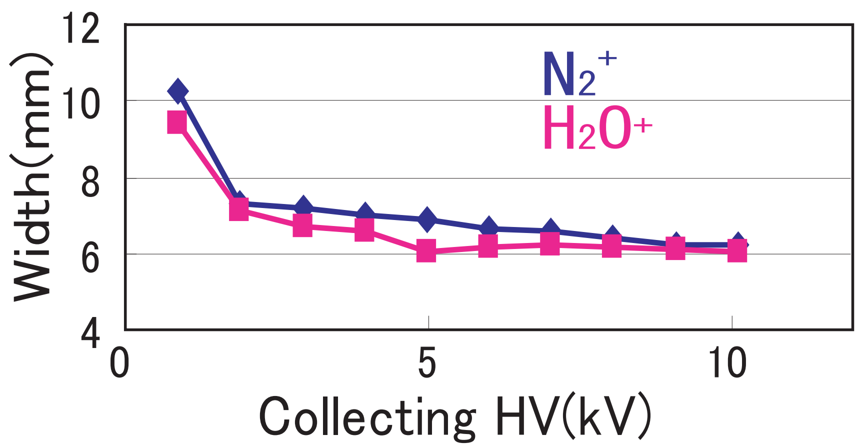

Figure 5.23: Collecting high voltage dependence of measured beam width.

5.5 Summary

We develop the Residual Gas Beam Profile Monitor for the J-PARC neutrino beamline. The number of the ionized particles of residual gas is small, then we select the multi-anode MCP as a readout device, which provides the large gain of over 10^6. In the J-PARC neutrino beamline, the beam induced electric field is so strong that a magnetic field is necessary for electrons to keep the information of initial position. While, the realistic magnetic field cannot keep the beam profile for the positive ion collection.

We carry out the beam test at K2K neutrino beamline in the KEK-PS. We try to measure the beam profile in a magnetic field. The electrodes collect electrons and the ADC gate is opened at the beam timing. There is too large background to measure the beam profile. We measure the beam loss around the monitor and find that the amount of the beam loss is much larger than that in other accelerators and beamlines. This strongly indicates the beam shower around the beamline hitting the MCP directly causes the large background of RGBPM.

Next, we carry out the second beam test at the NML beamline at KEK-PS. We measure the proton beam profile and study the basic performance of RGBPM. We find that the positive ion collection is necessary to avoid the beam induced background, since the signal timing for the positive ions is delayed from the beam timing about 1 microsecond. The effect of the beam induced electric field is also studied. We find that, if we use only the electric field to collect the positive ions, RGBPM works under the electric field produced by the proton beam up to 20kV/m, which is much smaller than the one at the J-PARC neutrino beamline. RGBPM is not suitable for the J-PARC neutrino beamline, though at the normal beamlines with much lower intensity, RGBPM can measure beam profiles using positive ion collection under the high beam background environment.

We have to develop another profile monitor for the final focusing section. We start to develop the Halo monitor as one of the next candidate.

Chapter 6

Conclusion

In the T2K experiment, the J-PARC neutrino beamline is one of the most important apparatus. Since the intensity of the proton beam is very high, the beam monitors are important for, especially, protecting the target from breaking. It is necessary to establish the beam tuning scheme to deliver the beam precisely, and to develop the profile monitor in front of the target. We study the positions of beam monitors and the beam tuning scheme, and study RGBPM as the beam profile monitor.

Beam Monitoring and Tuning Scheme

We perform the beamline simulations of the J-PARC neutrino beamline. In this simulations, we study the tuning scheme of the beam center position and check the validity of the positions and number of beam monitors and steering magnets. Assuming the resolution of the beam position measurement as 0.5mm, we find the accuracy of the beam position measurement at the target satisfies the requirement for the X direction, but does not satisfy for the Y direction since the final beam monitor is set 4m away from the target. It is required to put the monitor at less than 4m from the target, and/or to improve the resolution of the beam monitor.

The possibility of the emittance measurement at the preparation section is also checked. The accuracy of the measurement is estimated about 10% in both X and Y directions assuming the resolution of the profile monitor of ± 0.7mm. The measured emittance is used for the tuning of the quadrupole magnets and for the estimation of the beam size at the target. With the current configuration, the accuracy of the estimation of the beam size at the target is about 14%, to the contrary the required accuracy is 7%.

R&D of RGBPM

We also study the feasibility of the Residual Gas Beam Profile Monitor (RGBPM) as a non-destructive profile monitor for the J-PARC neutrino beamline. RGBPM performs as an alternate profile monitor of Segmented Secondary Emission Monitor to be installed in the final focusing section. The Micro Channel Plate is used as a read out device. From the result of the simulation, electron collection with a magnetic field of more than 0.05T is necessary to measure the beam profile. There are two beam tests of RGBPM at the K2K neutrino beamline and at the NML beamline in the KEK-PS.

In the first beam test, we try to check the basic performance of RGBPM under the magnetic field. The beam profile is not measured since there is a large background. The measurement of the beam loss around the detector strongly indicates the background is due to the beam halo and/or shower around the beamline.

In the second beam test, we measure the beam profile with positive ion collection mode. We find that the positive ion collection is necessary to avoid the beam induced background. The effect of the beam induced electric field is also studied. We find that, if we use only the electric field to collect the positive ions, RGBPM works under the electric field produced by the proton beam up to 20kV/m, which is much smaller than the one at the J-PARC neutrino beamline.

We concluded that RGBPM is not suitable for the J-PARC neutrino beamline, though RGBPM can measure beam profiles at the beamlines with much lower intensity than J-PARC, using the positive ion collection under the high beam background environment. As the alternative device to RGBPM, we have to develop other candidate monitors to get the beam size information for the final focusing section. Halo monitor and core-less LPM are considered as the profile monitors.

To summarize, we have established the positions of beam monitors and the tuning scheme of beam center in the preparation section. In the final focusing section, to measure the beam position and size precisely, we have to arrange the design around the target, and to develop a special monitor to measure the beam profile continuously. We find that RGBPM is not suitable as the monitor. We have to develop the spacial beam monitors to be installed near the target.

Acknowledgement

I would like to express my great appreciation to my supervisor H. Aihara. I am especially thankful to M. Iwasaki. I also show my appreciation to H. Kakuno. I would like to acknowledge T. Abe.

I am deeply thankful to KEK Beam Channel Group: H. Noumi, Y. Sato, A. Toyoda, E. Hirose, K. Agari, M. Ieiri, H. Takahashi, Y. Yamanoi and all the other members. I especially thank KEK Neutrino Group: A. Ichikawa, T. Kobayashi, Y. Hayato and all the other members. I am grateful NML Beamline Group: H. Fujimori, Y. Hashimoto, S. Muto.

I am thankful to M. Yokoyama, T. Nakadaira, T. Tomura, H. Kawai, N. Uozaki, Y. Yamashita, A. Kusaka, K. Tanabe for their kind advise. I also thank K. Itoh, Y. Nakahama, H. Nakayama.

Appendix A

Neutrino Oscillation

A.1 History of neutrino and its mass

In 1930s, Pauli predicted the existence of neutrinos to explain the β decay which seemingly broke the principle of conservation of energy. This is the opening of the history of neutrinos. After that, Fermi made the Four-Fermi Hamiltonian explaining the interaction of neutrinos, which was the theoretical foundation of neutrinos. In 1956, Reines and Cowan succeeded the experimental direct observation of neutrinos produced in the nuclear reactor. It turned out that these neutrinos were anti-electron neutrinos. Muon neutrinos and tau neutrinos, which were the other kinds of neutrinos, were directly observed in 1962 and in 1997, respectively. Moreover, the measurement of the Z boson's decay width, which was carried out at LEP accelerator, showed the number of kinds of neutrinos is three.

In our days, we use the standard theory to describe the phenomenon of elementary particles. The standard theory is very well in agreement with the various experiments. The description that neutrinos are massless particles is also supported with some experiments. The upper limits of the masses of the three neutrino species is as follows[17].

$$\begin{aligned} m_{\nu_e} &< 3\mathrm{eV} \\ m_{\nu_\mu} &< 190\mathrm{keV} \\ m_{\nu_\tau} &< 18.2\mathrm{MeV} \end{aligned}$$

However, recent atmospheric and solar neutrino experiments show that neutrinos have masses and large mixing. These properties cause the neutrino oscillation. We will describe the neutrino oscillation in the next section.

A.2 Neutrino oscillation

Neutrino oscillation is the phenomenon that a neutrino changes its flavor, caused by the mixing between the flavor eigenstate and the mass eigenstate, when the neutrino has a non-degenerate mass. The mixing of neutrinos is described as follows,

$$\begin{pmatrix} \nu_e \\ \nu_\mu \\ \nu_\tau \end{pmatrix} = \begin{pmatrix} U_{e1} & U_{e2} & U_{e3} \\ U_{\mu 1} & U_{\mu 2} & U_{\mu 3} \\ U_{\tau 1} & U_{\tau 2} & U_{\tau 3} \end{pmatrix} \begin{pmatrix} \nu_1 \\ \nu_2 \\ \nu_3 \end{pmatrix}$$

where ν_e, ν_μ, ν_τ are the flavor eigenstates and ν_1, ν_2, ν_3 are the mass eigenstates. The unitary matrix U is called MNS matrix (Maki-Nakagawa-Sakata matrix), which corresponds to CKM matrix (Cabbibo-Kobayashi-Masukawa matrix) in quark sector. The elements of the matrix U consist of four free parameters, three mixing angles θ_1, θ_2, θ_3 and CP violation phase δ.

$$U = \begin{pmatrix} 1 & 0 & 0 \\ 0 & c_{23} & s_{23} \\ 0 & -s_{23} & c_{23} \end{pmatrix} \begin{pmatrix} c_{13} & 0 & s_{13}e^{-i\delta} \\ 0 & 1 & 0 \\ -s_{13}e^{i\delta} & 0 & c_{13} \end{pmatrix} \begin{pmatrix} c_{12} & s_{12} & 0 \\ -s_{12} & c_{12} & 0 \\ 0 & 0 & 1 \end{pmatrix}$$

where $c_{ij} = \cos\theta_{ij}$ and $s_{ij} = \sin\theta_{ij}$.

Neutrinos are produced by weak interaction as flavor eigenstates. However, the time evolution of the states is described as the mass eigenstates and the Schrodinger equation is as follows,

$$i\frac{d}{dt}\nu_i(t) = H\nu_i(t)$$

where H is Hamiltonian. The energy eigenvalues of each mass eigenstate are

$$E_i = \sqrt{p^2 + m_i^2} \sim p + \frac{m_i^2}{2p}$$

assuming the momentum p is common. The equation can be solved as follows,

$$\nu_i(t) = \exp(-iE_i t)\nu_i(0)$$

The difference of the time evolution between three mass eigenstates causes the neutrino oscillation.

The probability that the ν_α at the time $t = 0$ changes its flavor to ν_β after finite time t is described as,

$$\begin{aligned} P(\nu_\alpha \to \nu_\beta) &= |\nu_\beta(t) \cdot \nu_\alpha(0)|^2 && \text{(A.1)} \\ &= \delta_{\alpha\beta} - 4\sum_{i<j} Re(U_{\alpha i}^* U_{\beta i} U_{\alpha j} U_{\beta_j}^*) \cdot \sin^2\Phi_{ij} \\ &\quad -2\sum_{i<j} Im(U_{\alpha i}^* U_{\beta i} U_{\alpha j} U_{\beta_j}^*) \cdot \sin 2\Phi_{ij} && \text{(A.2)} \end{aligned}$$

where

$$\Phi_{ij} \equiv \Delta m_{ij}^2 L/4E_\nu = 1.27\Delta m_{ij}^2[eV^2]L[km]/E_\nu[GeV], \tag{A.3}$$

$\Delta m_{ij}^2 = m_j^2 - m_i^2$,$L$ is the neutrino flight distance ($\sim t$), and E_ν is the neutrino energy ($\sim p$).

According to the solar and atmospheric neutrino experiment mentioned in following sections, $\Delta m_{12}^2 \ll \Delta m_{13}^2 \sim \Delta m_{23}^2$. Using these results, the oscillation probabilities can be expressed by the following.

$$P(\nu_\mu \to \nu_\mu) \sim 1 - \cos^4\theta_{13}\sin^2 2\theta_{23}\sin^2\Phi_{23} \tag{A.4}$$
$$P(\nu_\mu \to \nu_e) \sim \sin^2\theta_{13}\sin^2\theta_{23}\sin^2\Phi_{23} \tag{A.5}$$

These give the oscillation pattern depending on the neutrino flight distance L and the energy E_ν.

The observation of neutrino oscillation proves the fact that at least one flavor neutrinos have finite masses. Various neutrino oscillation experiments have been performed to find the oscillation. They are explained in following sections.

A.3 Neutrino oscillation experiment

A.3.1 Atmospheric neutrino experiment

Atmospheric neutrinos are produced by the decay of pions, kaons and muons. The interaction of primary cosmic rays from the universe with the upper atmosphere creates the hadronic showers. The produced pions and kaons decay to muons and muon neutrinos. Further, the muons decay to electrons, muon neutrinos and electron neutrinos. The decay chain is as following:

$$\begin{aligned} p + X &\rightarrow \pi^\pm/K^\pm + X' \\ \pi^\pm/K^\pm &\rightarrow \mu^\pm\nu_\mu(\overline{\nu_\mu}) \\ \mu^\pm &\rightarrow e^\pm\overline{\nu_\mu}\nu_e(\nu_\mu\overline{\nu_e}). \end{aligned}$$

The expected flux ratio $\nu_\mu+\overline{\nu_\mu}/\nu_e+\overline{\nu_e}$ is 2. The ratio is predicted with an uncertainty of less than 5%. It has been measured by several experiments: Kamiokande, IMB, Super-Kamiokande and Soudan-2. These experiments report that the ratio is significantly smaller than that of the Monte Calro Simulation. The results suggest the neutrino oscillations.

From the result of Super-Kamiokande, the allowed region of $\sin^2\theta_{23}$ and Δm^2 is shown in Fig.A.1.

A.3.2 K2K long baseline neutrino oscillation experiment

The KEK to Kamioka long baseline neutrino experiment (K2K experiment) is the first accelerator neutrino experiment with hundreds of kilometers neutrino path length. The existence of neutrino oscillations can be confirmed very clearly since the neutrino flux and their flavor is well known.

In the K2K experiment, a muon neutrino beam is produced by the 12GeV KEK-PS proton beam. The neutrino beam is detected by Super-Kamiokande located 250km away from the KEK. Its result is shown as the indication of the neutrino oscillation [2].

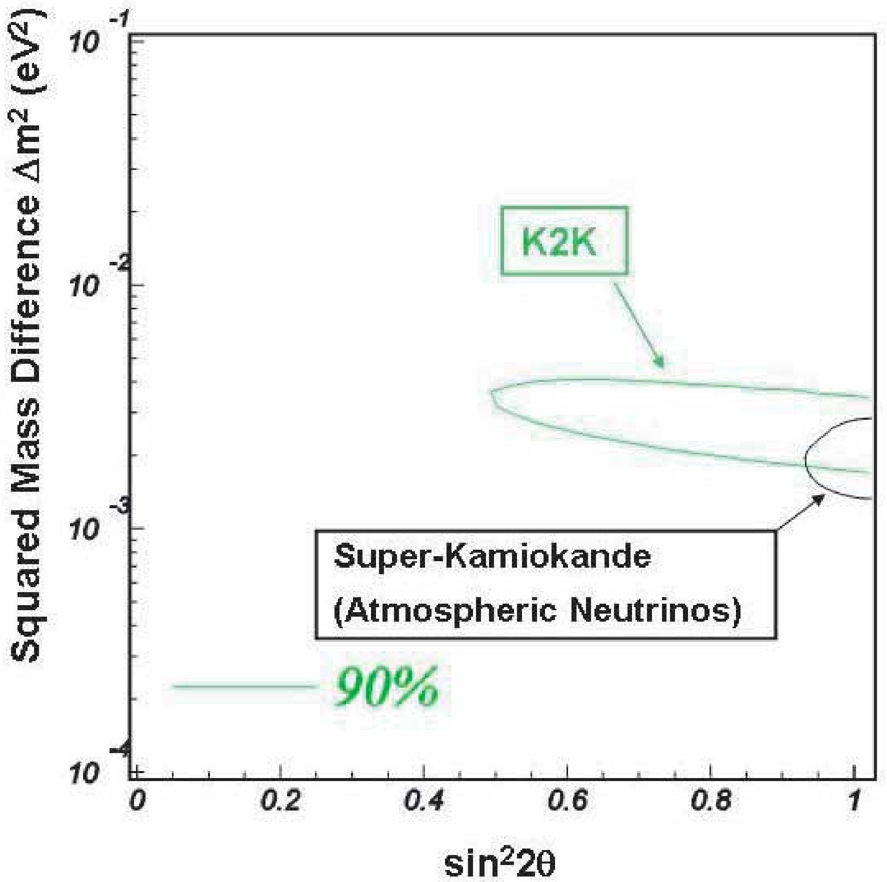

Figure A.1: Contours enclosing the 90% confidence reagions for the neutirno oscillation parameters. The black and green lines corresponds to the results from Super-Kamiokande atmospheric neutrino experiment and those from the K2K accelerator neutrino experiment, respectively.

Appendix B

Linear Beam Optics

Here we describe the linear beam optics [18] used in our simulation study of the emittance measurement. The beam size evolution is determined by the emittance ϵ, the twiss parameters α, β, γ. The emittance is the parameter which the beam itself has, and is unchanged for all the beamline unless the beam is accelerated. The twiss parameters are the parameters which the beamline has, and its evolution is expressed only by the transfer matrix of the beamline components (See B.2). There is a relation among three parameters,

$$\gamma = \frac{1+\alpha^2}{\beta} \tag{B.1}$$

and then, the number of free parameters are two.

B.1 Expression of the Beam Size

Fig.B.1 shows an example of a beam phase space ellipse. Each particle is in the ellipse whose area is equal to $\epsilon\pi$. The maximum point of the ellipse is expressed as $\sqrt{\epsilon\beta}$ in the position axis, and $\sqrt{\epsilon\gamma}$ in the direction axis. We can measure only $\sqrt{\epsilon\beta}$ as a maximum beam size.

Assuming the particles are distributed uniformly in the ellipse, as is assumed in Section 3.5, the beam profile function is expressed as $f(x) = \sqrt{A - Bx^2}$. A and B are free parameters and the beam size is expressed as follows,

$$\sqrt{\epsilon\beta} = \sqrt{\frac{A}{B}} \equiv x_0. \tag{B.2}$$

The RMS (Root Mean Square) of the beam profile distribution is calculated as

$$\mathrm{RMS} = \frac{\int_{-x_0}^{x_0} x^2 f(x)}{\int_{-x_0}^{x_0} f(x)} = \frac{x_0}{2}. \tag{B.3}$$

The beam profile size is also expressed as $2\times$RMS.

But in the actual beam, the measured beam size depends on the many factors like the shape of the distribution, the definition of the beam size and so on. We have to use a collective definition of the beam size.

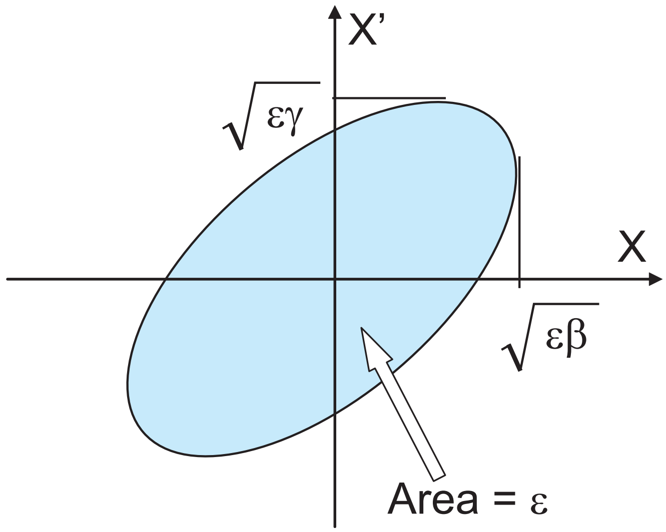

Figure B.1: A phase space of a beam.

B.2 Twiss Parameter Evolution and Transfer Matrix

We describe how to determine the evolution of the twiss parameters along the orbit of the beamline. We assumed that the values of the twiss parameters at a given initial point are known. Starting from this initial point, the twiss parameters can be calculated step by step along the structure of the magnets by the transfer matrix.

The beta matrix at the initial point ($s = s_0$)is defined as

$$B_0 \equiv \begin{pmatrix} \beta_0 & -\alpha_0 \\ -\alpha_0 & \gamma_0 \end{pmatrix} \tag{B.4}$$

The beta matrix at the point $s = s_1$ is written as

$$B_1 = M \cdot B_0 \cdot M^T \tag{B.5}$$

where the matrix M is the transfer matrix from s_0 to s_1.

The transfer matrix of each component is determined as follows,

- Drift Space

$$M = \begin{pmatrix} 1 & s \\ 0 & 1 \end{pmatrix} \tag{B.6}$$

  where s is the length of a component (same with all other components).

- Dipole magnet for the bending direction

$$M = \begin{pmatrix} \cos\frac{s}{R} & R\sin\frac{s}{R} \\ -\frac{1}{R}\sin\frac{s}{R} & \cos\frac{s}{R} \end{pmatrix} \tag{B.7}$$

  where $\frac{1}{R}$ is a curvature radius ($= \frac{e}{p} \cdot B$). For the non-bending direction, the transfer matrix is identical to that for the drift space.

- Edge effect of a bending rectangular magnet

$$M = \begin{pmatrix} 1 & 0 \\ \dfrac{\tan\Psi}{R} & 1 \end{pmatrix} \text{for the bending direction} \tag{B.8}$$

$$M = \begin{pmatrix} 1 & 0 \\ -\dfrac{\tan\Psi}{R} & 1 \end{pmatrix} \text{for the non} - \text{bending direction} \tag{B.9}$$

where Ψ is a half of the bending angle of the dipole magnet.

- Quadrupole magnet
By the definition $k = \frac{e}{p}\frac{dB}{dx}$,

$$M = \begin{pmatrix} \cos\Omega & \dfrac{1}{\sqrt{|k|}}\sin\Omega \\ -\sqrt{|k|}\sin\Omega & \cos\Omega \end{pmatrix} \text{for } k > 0 \text{ (defocusing)} \tag{B.10}$$

$$M = \begin{pmatrix} \cosh\Omega & \dfrac{1}{\sqrt{|k|}}\sinh\Omega \\ \sqrt{|k|}\sinh\Omega & \cosh\Omega \end{pmatrix} \text{for } k < 0 \text{ (focusing)} \tag{B.11}$$

where $\Omega = \sqrt{|k|}s$

The combination transfer matrix of more than one component can be written as $M = M_n \cdot M_{n-1} \cdot \cdots \cdot M_1$.

We introduce another expression of the twiss parameters' evolution. Assuming the transfer matrix M is expressed as:

$$M = \begin{pmatrix} m_{11} & m_{12} \\ m_{21} & m_{22}, \end{pmatrix} \tag{B.12}$$

the relation of twiss parameters between $s = s_0$ and $s = s_1$ can be given as

$$\begin{pmatrix} \beta_1 \\ \alpha_1 \\ \gamma_1 \end{pmatrix} = \begin{pmatrix} m_{11}^2 & -2m_{11}m_{12} & m_{12}^2 \\ -m_{11}m_{21} & m_{11}m_{22} + m_{12}m_{21} & -m_{22}m_{12} \\ m_{21}^2 & -2m_{22}m_{21} & m_{22}^2 \end{pmatrix} \begin{pmatrix} \beta_0 \\ \alpha_0 \\ \gamma_0 \end{pmatrix} \tag{B.13}$$

For example, the β function evolution in the drift space is expressed as a second-degree function of $s = s_1 - s_0$;

$$\beta_1 = \beta_0 - 2s\alpha_0 + s^2\gamma_0 \tag{B.14}$$

This indicates the square of the beam size ($= \epsilon\beta$) is a second-degree function of the orbit length in a drift space.

The momentum dispersion ($\Delta p/p \neq 0$) must also be considered for the calculation of the particle trajectory. A particle whose momentum is different from the design momentum deviates from the design orbit since the bending angle in magnets is different. The η function is defined as a trajectory for $\Delta p/p = 1$. The η function is also calculated using the transfer matrix of the beamline components. The $\Delta p/p$ is determined by the accelerator as a beam parameter.

The beam size with the non-zero momentum dispersion is wider than the beam size without the dispersion. It is difficult to define the beam size as a formula, but the following expression is often used.

$$w = \sqrt{\epsilon\beta + (\eta\frac{\Delta p}{p})^2} \tag{B.15}$$

Bibliography

[1] Super-Kamioaknde collaboration “Evidence for Oscillation of Atmospheric Neutrinos” *Phys.Rev.Lett.* 81,1562 (1998)

[2] The K2K collaboration “Indication of Neutrino Oscillation in a 250km Long-baseline Experiment” *Phys.Rev.Lett.* 90,041801 (2003)

[3] Super-Kamioaknde collaboration “Tau Neutrinos Flavored over Sterile Neutrinos in Atmospheric Muon Neutrino Oscillations” *Phys.Rev.Lett.* 85,3999 (2000)

[4] Super-Kamioaknde collaboration “Solar ^{8}B and hep Neutrino Measurement from 1258 Days of Super-Kamiokande Data” *Phys.Rev.Lett.* 86,5651 (2001)

[5] “Letter Of Intent, Neutrino Oscillation Experiment at JHF”, http://neutrino.kek.jp/jhfnu (Jan,2003)

[6] Y. Hayato et al. “J-PARC Neutrino Facility Technical Design & Development (Interim) Report”

[7] S. Agostinelli et al. “GEANT4-a simulation toolkit” *Nuclear Instruments and Methods A* 506,250 (2003)

[8] A. R. Berdoz et al. “A beam intensity profile monitor based on secondary electron emission”, *Nuclear Instruments and Methods A* 307,26 (1991)

[9] K. H. Tanaka et al. “Improvement in the Profile and Emittance Measurement System of the KEK-PS External Beam Line”, *KEK-Preprint* 91-27 (May,1991)

[10] K. Sato “Emittance measurement at the 500MeV Beam Transport Line” (Japanese), *KEK-PS Accelerator Study Note* ASN-144 (Oct,1978)

[11] S. Ueda Master Thesis (Japanese), (2003)

[12] T. Kawakubo et al. “Non-Destructive Beam Profile Monitors in the KEK Proton Synchrotron”, KEK Preprint 91-23

[13] R. Connolly et al. “The RHIC Ionization Beam Profile Monitor”, Proceedings of the 1999 Particle Accelerator Conference, (1999)

[14] J. Krider “Residual Gas Beam Profile Monitor”, *Nuclear Instruments and Methods A* 278,660 (1989)

[15] Hamamatsu Photonics K. K., "PHOTOMULTIPLIER TUBE -the foundation and application"

[16] Hamamatsu Photonics K. K., "MCP Assembly Technical Data"

[17] Particle Data Group (2004)

[18] K. Wille "The Physics of Particle Accelerators -an introduction", Oxford University Press (2000)